

University of Windsor

Scholarship at UWindor

Electronic Theses and Dissertations

Theses, Dissertations, and Major Papers

2022

Analysis of Combustion in Plasma Electrolytic Oxidation (PEO) Coatings of the Piston Surface in Spark Ignition Engines

Brendon Bain
University of Windsor

Follow this and additional works at: <https://scholar.uwindsor.ca/etd>



Part of the [Automotive Engineering Commons](#), and the [Mechanical Engineering Commons](#)

Recommended Citation

Bain, Brendon, "Analysis of Combustion in Plasma Electrolytic Oxidation (PEO) Coatings of the Piston Surface in Spark Ignition Engines" (2022). *Electronic Theses and Dissertations*. 9007.
<https://scholar.uwindsor.ca/etd/9007>

This online database contains the full-text of PhD dissertations and Masters' theses of University of Windsor students from 1954 forward. These documents are made available for personal study and research purposes only, in accordance with the Canadian Copyright Act and the Creative Commons license—CC BY-NC-ND (Attribution, Non-Commercial, No Derivative Works). Under this license, works must always be attributed to the copyright holder (original author), cannot be used for any commercial purposes, and may not be altered. Any other use would require the permission of the copyright holder. Students may inquire about withdrawing their dissertation and/or thesis from this database. For additional inquiries, please contact the repository administrator via email (scholarship@uwindsor.ca) or by telephone at 519-253-3000ext. 3208.

Analysis of Combustion in Plasma Electrolytic Oxidation (PEO) Coatings of the Piston Surface in Spark Ignition Engines

By

Brendon Bain

A Thesis
Submitted to the Faculty of Graduate Studies
through the Department of Mechanical, Automotive & Materials Engineering
in Partial Fulfillment of the Requirements for
the Degree of Master of Applied Science
at the University of Windsor

Windsor, Ontario, Canada

2022

© 2022 Brendon Bain

**Analysis of Combustion in Plasma Electrolytic Oxidation (PEO) Coatings of the Piston
Surface in Spark Ignition Engines**

by

Brendon Bain

APPROVED BY:

N. Kar

Department of Electrical and Computer Engineering

J. Tjong

Department of Mechanical, Automotive & Materials Engineering

X. Nie, Co-Adviser

Department of Mechanical, Automotive & Materials Engineering

M. Zheng, Co-Adviser

Department of Mechanical, Automotive & Materials Engineering

August 29, 2022

DECLARATION OF ORIGINALITY

I hereby certify that I am the sole author of this thesis and that no part of this thesis has been published or submitted for publication.

I certify that, to the best of my knowledge, my thesis does not infringe upon anyone's copyright nor violate any proprietary rights and that any ideas, techniques, quotations, or any other material from the work of other people included in my thesis, published or otherwise, are fully acknowledged in accordance with the standard referencing practices. Furthermore, to the extent that I have included copyrighted material that surpasses the bounds of fair dealing within the meaning of the Canada Copyright Act, I certify that I have obtained a written permission from the copyright owner(s) to include such material(s) in my thesis and have included copies of such copyright clearances to my appendix.

I declare that this is a true copy of my thesis, including any final revisions, as approved by my thesis committee and the Graduate Studies office, and that this thesis has not been submitted for a higher degree to any other University or Institution.

ABSTRACT

With the global effort to “green” the transportation industry, the internal combustion engine (ICE) is required to reduce its carbon footprint and can do so by increasing efficiency. Plasma Electrolytic Oxidation (PEO) coatings confer properties of high wear and corrosion resistance, high hardness, excellent adhesion and a superior thermal barrier to their substrate, suggesting that coating of ICE components has the potential to greatly improve the combustion efficiency. The primary objective of this thesis is to analyze the effects of PEO coating on the surface of pistons in a spark ignition ICE, with the goal of increasing efficiency, to address the industry targets of reduced carbon emissions and increase fuel efficiency.

Testing was conducted on a 7.3L Ford engine fitted with stock Al alloy pistons, followed by in-house PEO-coated pistons. An AC Medien dynamometer and a A&D Pheonix AM/RT combustion analysis system using real-time in-cylinder pressure data, coupled with the dynamometer cell data were used. The testing was built off real world driving cycles overlaid on a brake specific fuel consumption (bsfc) map, to choose areas upon which to focus during the completion of the spark and VCT timing sweeps at both, low load and high load conditions.

Compared to stock pistons, the PEO-coated pistons modestly improved bsfc, thermal efficiency, increased HRR and bulk gas temperature at low load, low speed conditions. These benefits did not project further onto retarded VCT angles and higher speeds, where PEO-coated pistons did not change thermal efficiency, bsfc, had minimal impact on bulk gas temperatures, and minimally influenced the IMEP COV. At high load and speed conditions the PEO-coating negatively impacted the engine performance, inducing knock. An increased fuel enrichment was required to reduce exhaust temperature limits, since retarding spark was required to reduce knocking. The engine could not be run at optimum efficiency or MBT spark timing, decreasing the bsfc and thermal efficiency.

In conclusion, although benefit derived from the use of PEO-coated pistons was observed only in limited engine conditions, the data collected and analyzed in this thesis provides a direction for future study to continue to explore the potential advantages of PEO-coated pistons.

ACKNOWLEDGMENTS

I would like to thank my supervisors Dr. Xueyuan Nie and Dr. Ming Zheng for all their support throughout the duration of my Masters program. Their direction and assistance were very helpful with the completion of my study. I would additionally like to thank my work colleagues and friends Dr. Usman Asad, Dr. Prasad Divekar, Dr. Xiaoye Han, and Guang Wang for all their suggestions, directions and support provided during my work on my project. I am indebted to, and thank my friend and work supervisor Xiaoxi Zhang, for his support and for facilitating additional time for me to work on my thesis. I would like to thank my boss and external committee member, Dr. Jimi Tjong, for his guidance, and supplying of equipment required for this project. I would like to thank Power Train Research and Development Center, PERDC, and the Ford Motor Company for use of their facilities while completing this Masters thesis. I would like to thank Simon Leblanc for the assistance with this project and programing code.

TABLE OF CONTENTS

DECLARATION OF ORIGINALITY	iii
ABSTRACT.....	iv
ACKNOWLEDGMENTS	v
LIST OF TABLES	viii
LIST OF FIGURES	ix
NOMENCLATURE	xi
CHAPTER 1 INTRODUCTION	1
1.1 Research Background.....	1
1.2 PEO Coatings	2
1.3 Coating Process.....	4
1.4 Research Objectives	5
CHAPTER 2 LITERATURE REVIEW	7
2.1 Literature Review Objectives and Overview	7
2.2 Coating Methods	7
2.3 Coating Applications.....	14
CHAPTER 3 EXPERIMENTAL DETAILS	19
3.1 Engine Setup	19
3.2 Process for Coating the Pistons.....	22
3.3 Dynamometer Cell Setup	26
3.4 Combustion Analysis System (CAS) Setup.....	27
3.5 Test Setups	29
3.6 Quality Checks	32
CHAPTER 4 EXPERIMENTAL RESULTS	35
4.1 Data Processing.....	35
4.2 PEO Coated Piston Inspection following Completion of Testing	38
4.2 Low Load Analysis and Experimental Results	39
4.3 High Load Analysis and Experimental Results	50
CHAPTER 5 CONCLUSIONS AND RECOMMENDATIONS	58

5.1 Conclusions	58
5.2 Recommendations for Future Work.....	59
REFERENCES	62
APPENDIX.....	67
VITA AUCTORIS	75

LIST OF TABLES

Table 3.1 – Engine specifications	20
Table 3.2 - Engine temperature and pressure control parameters.....	22
Table 3.3 – Selected low load spark sweep and VCT sweep points.....	32
Table 3.4 - Selected high load spark sweep and VCT sweep points	32
Table 4.5 - Steady-state results summary 1000rpm 5° VCT retard low load	41
Table A.6 - Steady-state results summary 1500rpm 50° VCT retard low load	71

LIST OF FIGURES

Figure 3.1 - Engine and dynamometer cell setup and instrumentation.....	21
Figure 3.2 - Voltage and current versus time for the DC pulsed PEO coating method represented as an absolute.....	23
Figure 3.3 - Stock piston and cover for coating process.....	24
Figure 3.4 - Electrolyte solution tank during the coating process and coated piston	25
Figure 3.5 - PEO coated piston finished product.....	26
Figure 3.6 - Kistler cylinder pressure transducers and installation location.....	28
Figure 3.7 - Cylinder pressure traces showing knocking vs no knock combustion cycle events .	29
Figure 3.8 - Mini-map points and transient test cycle overlaid on a bsfc map	31
Figure 3.9 - Data collection flow diagram	32
Figure 3.10 - Volume vs Theta graph	33
Figure 3.11 - Log p vs Log V graph for cylinder pressure data quality check	34
Figure 4.12 - Piston underside after testing completion	39
Figure 4.13 - Thermal efficiency versus spark advance at 1000 rpm 5° VCT retard	41
Figure 4.14 - bsfc vs spark advance at 1000rpm 5° VCT retard	42
Figure 4.15 - Heat Release Rate at 1000rpm 5° VCT retard spark sweep	43
Figure 4.16 - Bulk Gas temperature at 1000rpm 5° VCT retard spark sweep.....	44
Figure 4.17 - Log p vs Log V at 1000rpm at 5° VCT retard spark sweep.....	45
Figure 4.18 - Combustion duration coated piston vs uncoated at 1000rpm 5deg VCT retard spark sweep	46
Figure 4.19 - IMEP COV coated piston vs stock piston spark sweep at 1000rpm 5° VCT retard.....	47
Figure 4.20 - Thermal efficiency versus spark advance at 1500 rpm 50° VCT retard	48
Figure 4.21 - Bulk Gas temperature at 1500rpm 50° VCT retard spark sweep.....	49
Figure 4.22 - IMEP COV coated piston vs stock piston spark sweep at 1500rpm 50° VCT retard.....	50
Figure 4.23 - Stock piston underside	52
Figure 4.24 - Knock peak-to-peak 3500rpm full/high load 5° VCT retard	53
Figure 4.25 - Knock peak-to-peak 4000rpm full/high load 15° VCT retard	53
Figure 4.26 - Knock peak-to-peak 3500rpm full/high load 10° VCT retard	54
Figure 4.27 - Heat Release Rate at 3500rpm 10° VCT retard full load spark sweep	56

Figure 4.28 - Cylinder pressure traces at 3500rpm 10° VCT retard spark sweep	56
Figure 4.29 - Estimated thermal efficiency extrapolated at 3500rpm 10° VCT full load	57
Figure A.30 - A&D Phoenix CAS hardware and Kistler MAP sensor amplifier	67
Figure A.31 - AC Meiden dynamometer	68
Figure A.32 - AVL encoder and mounting bracket	69
Figure A.33 - bsfc vs spark advance at 1500rpm 50° VCT retard.....	70
Figure A.34 - Heat Release Rate at 1500rpm 50° VCT retard spark sweep, Cylinder #1.....	70
Figure A.35 - Heat Release Rate at 1500rpm 50° VCT retard spark sweep, Cylinder #2.....	71
Figure A.36 - Heat Release Rate at 1500rpm 50° VCT retard spark sweep, Cylinder #3.....	72
Figure A.37 - Heat Release Rate at 1500rpm 50° VCT retard spark sweep, Cylinder #4.....	72
Figure A.38 - Heat Release Rate at 1500rpm 50° VCT retard spark sweep, Cylinder #5.....	73
Figure A.39 - Heat Release Rate at 1500rpm 50° VCT retard spark sweep, Cylinder #6.....	73
Figure A.40 - Heat Release Rate at 1500rpm 50° VCT retard spark sweep, Cylinder #7.....	74
Figure A.41 - Heat Release Rate at 1500rpm 50° VCT retard spark sweep, Cylinder #8.....	74

NOMENCLATURE

AFR	Air to Fuel Ratio
Al	Aluminum
AM	Air Mass
ATDC	After Top Dead Center
bsfc	Brake Specific Fuel Consumption
BTDC	Before Top Dead Center
Bulk Gas Temp	Bulk Gas Temperature
CAS	Combustion Analysis System
Cu	Copper
EA	Engine Average
EDS	Dispersive X-ray spectroscopy
EFI	Electronic Fuel Injection
EGR	Exhaust Gas Recirculation
EPA	Environmental Protection Agency
HVOF	High Velocity Oxygen Fuel
HRR	Heat Release Rate
ICE	Internal Combustion Engine/Engines
IMEP	Indicated Mean Effective Pressure
LHV	Lower Heating Value
MAP	Manifold Pressure Sensor
MBT	Maximum Brake Torque
Mg	Magnesium
NO _x	Nitrogen Oxides
NVH	Natural Vibration Harmonics
PCM	Powertrain Control Module
PEC	Plasma Electrolytic Carburizing

PED	Plasma Electrolytic Deposition
PEN	Plasma Electrolytic Nitriding
PEO	Plasma Electrolytic Oxidation
PES	Plasma Electrolytic Saturation
PFI	Port Fuel Injection
PMEP	Pumping Mean Effective Pressure
PTWA	Plasma Transferred Wire Arc
RT	Real-Time
RTWA	Rotating Twin Wire Arc
SI	Spark Ignition
Spark Adv	Spark Advance
STD	Standard Deviation
Thermal_Eff	Thermal Efficiency
Ti	Titanium
TDC	Top Dead Center
VCT	Variable Cam Timing
YSZ	Yttria Stabilized Zirconia
Zn	Zinc

CHAPTER 1 INTRODUCTION

1.1 Research Background

The internal combustion engine (ICE) must increase its efficiency and reduce its carbon footprint to comply with future Environmental Protection Agency (EPA) regulations. The EPA stated future targets for 2026 fuel economy will be changed to 40mpg or 5.8L/100km compared to the current 32-36mpg or 7.3-6.5L/100km fleet average requirements [1]. Since the transportation sector is the largest greenhouse gas emitting sector in the USA and the second largest sector globally, it is necessary to increase ICE efficiency or find an alternative method to power our transportation [2, 3]. Electrification is a viable solution for the light-duty vehicle segment, but not for commercial vehicles, trains or trucks. Therefore, ICEs need to utilize alternative fuels to meet future emission regulations, pair-up with electrification or increase its efficiency. With electrification still presenting large hurdles to overcome with respect to charging infrastructure, range, remote location accessibility, and reliable heavy metal supply for sustainable battery production, increasing ICE efficiency is an alternative and viable solution.

This thesis evaluates the effect of Plasma Electrolytic Oxidation (PEO) Coatings on the piston surface or piston crown of a spark ignition (SI) engine. The study assesses the process of coating piston surfaces, the instrumentation set-up required for testing such as sensors, and analyze the combustion differences between coated and non-coated pistons. Using in-cylinder pressure data in conjunction with dynamometer cell data, the combustion cycles are analyzed to characterize the effects of the coating on different engine conditions. Since the piston is the only ICE component coated for this study, the analysis of the combustion cycle is simplified. The heat transfer to the cylinder walls and cylinder head are assumed to remain constant. The piston surface is also a large area of heat dissipation in the combustion chamber. There is limited research on the effect of coating the piston surface with ceramic-like coatings of SI port fuel injected (PFI) engines with variable camshaft timing (VCT) capability. Hardware differences and combustion chamber design are other variables that impact efficiency and have been studied but are not assessed in this project. Increased efficiencies of the intake manifold design, cylinder heads and in-cylinder swirl or tumble have also been demonstrated to impact the potential of PEO coatings.

The heat loss or heat transfer is one of the fundamental reasons for the inefficiency of internal combustion SI engines. The production standard average thermal efficiency for SI gasoline engines is between 20% - 35%, meaning there is approximately 65% - 80% wasted energy. Therefore, the goal is to reduce the heat transfer between the working gas to the combustion chamber components, or as in this study specifically, the piston. The reduced heat transfer will, theoretically, allow for more work to be extracted and with higher bulk gas temperatures exhausted, there is increased potential for energy recovery through the use of turbo charging or faster catalytic converter light off potential, reducing harmful cold start emissions. Work has been previously done by the US military focusing on the thermal properties of various coatings, with the aim to reduce heat transfer, allowing smaller cooling systems to increase the overall vehicle efficiency [4, 5, 6]. The observed properties of PEO coatings have encouraged research into their potential uses and applications. The present work analyzes the PEO-coating on a SI electronic fuel injection (EFI) multiport fuel engine with VCT capability. This study demonstrates the potential benefits of PEO coatings, enabling the ICE to continue supporting the transportation industry, by increasing efficiency and complying with future EPA regulations.

1.2 PEO Coatings

PEO coatings are hard, dense, wear-resistant and well-adhered oxide coatings that involve the modification of conventional anodically grown oxide films. The application of an electric field, greater than the dielectric breakdown field for the oxide, produces a coating of ceramic-like properties. During the application of the electrical field, a plasma-chemical reaction occurs and when discharging occurs, the growth of the coating propagates. The PEO coating process of forming oxide layers on Al, Ti and Mg alloys is based on the anodic oxidation in aqueous solutions with the application of the voltage exceeding the breakdown voltage of the developing oxide layer on the surface of the metal [7, 8, 9]. The coatings largely consist of a relatively dense polycrystalline layer of alpha-alumina with a softer more porous layer of gamma-alumina formed on the top [10, 11]. These layers can vary in thickness, structure, density and number of layers depending on the system setup, the material choice and the electrolyte composition.

The benefits of PEO coatings include high wear resistance, low friction, good corrosion resistance, high hardness, excellent adhesion, good heat resistance and low thermal conductivity. The coating properties are highly adjustable based on the electrolyte composition and properties, and the

electric regime chosen, which is discussed in detail in Section 2.2. The result is a large range of adjustability in targeting different coating properties for the intended application.

PEO coatings have a high wear resistance that is superior to other types of coatings or anodizing, such as hard anodizing, when the application process is completed correctly. PEO coatings also offer a low coefficient of friction of 0.5 with respect to itself when dry, and 0.1 when wet. The lower coefficient of friction when wet results in part from its porous surface structure, which can increase oil retention and consequently reduce the friction between two rubbing surfaces. However, while desirable with respect to lowering friction and improving heat transfer properties of the coating (see below), porosity can have negative effects on durability [12] .

PEO coatings are extremely corrosion resistant and can withstand 7000 hours in a salt-fog test chamber due, in part, to their charge transfer resistance. The charge transfer resistance of a PEO-coated surface is approximately 300 k Ω , compared to, for example, 5 k Ω for a bare aluminum surface. This results in a much greater resistance to the current flow, correlating to reduced corrosive attacks [13]. PEO coatings also have a very high hardness with a Vickers Number (HV) of 1400 – 1700 HV, where HV can also be represented as kilogram-force per square millimeter (kgf/mm²). Component hardness is important in ICEs to ensure the coating does not deteriorate during combustion. Moreover, PEO coatings adhere well to the substrate on which it forms, as long as the coating process is completed correctly. When the oxide layer is forming it permeates into the substrate, while simultaneously growing outwards away from the substrate surface, resulting in an extremely strong adhesion, which is discussed in detail in Section 2.2. PEO coatings can also withstand several seconds at the high temperatures of 2000°C without undergoing any change or deformation, which is critical for reliable performance in a combustion chamber.

PEO coatings have good insulating properties with a very low thermal conductivity of the order of 1 W/mK. This provides a good thermal barrier protecting the underlying substrate. In contrast, typical stock aluminum pistons, depending on the alloy compound, have a thermal conductivity in the order of 96 W/mK to 121 W/mK, allowing for significant heat transfer through the piston. The PEO coating would therefore reduce the thermal stress transferred to combustion chamber components [14]. Piston squirters are required on engines to help reduce and regulate the heat conducted through the piston during the combustion process. PEO coatings, by mitigating the thermal stress, would in turn reduce the cooling system capacity requirements. Thus, the

components' weight and thickness could potentially be reduced, thereby reducing overall engine weight [14]. Finally, PEO coatings also have good electrical resistance properties and research is ongoing to evaluate the capabilities of the coating as an electrical insulator [12].

1.3 Coating Process

PEO coating process consists of multiple stages: analyzing the material properties of the surface to be coated, preparation of the surface, choosing the electric regime, electrolyte composition and surface finishing after the coating process is completed. PEO coatings are most commonly applied to pure or alloyed Al, Ti or Mg metals, as the oxide forms best on those materials. However, PEO coatings have also been applied to iron-based materials and Copper (Cu) metals with less favorable results. Iron-based materials tend to exhibit poor passivation behavior and Cu particles tend to obstruct the conversion of the substrate during the oxidation process [13].

The preparation requirements of the surface of the substrate to be coated changes based on the electric regime and electrolyte solution chosen, but generally minimal preparation is required. Minimal preparation requirements consist of cleaning with acetone and ethanol, preferably in an ultrasonic cleaner for a machined component with uniform surface properties, and finally rinsing with distilled water. If the substrate surface is rough, non-machined or non-uniform, further surface preparation may be required such as grinding, sanding and polishing to ensure a uniform surface [7, 15]. Furthermore, etching and brightening preparation may be required to ensure a homogeneous well bonded oxide coating [7].

Selecting the electric regime and electric regime control factors for the coating process is important as the coating porosity, density, hardness, adhesion and corrosion resistance can all be influenced [16]. AC, DC, pulsed AC or DC, bipolar AC or DC or unipolar electric regimes can be chosen [7, 12, 13, 15, 17]. For an AC system, amperage spikes are used for the coating process to assist with the discharge of the electrolytes. The DC pulsed method uses a similar electric application by adjusting the frequency of the square wave lengths and intensity. For all PEO coating methods, the voltage application is initiated at a low setpoint and then increased as the process progresses because as the coating thickness increases so does the electrical resistance. An increased voltage is required to continue the growth of the coating as it thickens. The electrolyte composition drastically affects the coating properties because as the dielectric breakdown occurs the electrolyte

is deposited onto the surface of the substrate forming oxide layer [18]. The coating contains components of the electrolyte and the substrate. These factors affect the coating properties in different electric fields such that the coating process is highly adjustable and the coating properties are modular [19].

After the coating process is completed, the finishing process varies based on the intended application. Generally smoothing or polishing is required with the use of very fine wet sanding to remove rough spots or burs followed by rinsing in distilled or de-ionized water. Other applications require further sealing of the porous surface with the use of silicate spray [3] and if coatings are applied to cylinder bores, honing of the surface is required.

The discharging process produces a large amount of heat and as the heat of the electrolyte solution rises, the adhesion force to the substrate reduces. The electrolyte solution temperature must therefore be modulated to ensure a high-quality coating is produced with low roughness. To ensure the solution temperature is regulated, the electrolyte container needs to be cooled by an indirect heat exchanger. To assist with reduction of temperature during coating, blocking off or masking the areas that are not required to be coated, through the use of a plastic or non-conductive material, is necessary. The quality of the coating finish is also related to the voltage and current inputs, where the porosity increases with the current and the discharge is larger. However, with a higher current and larger discharge the density of the coating will be greater. Thus, the coating process requires a precise and accurate control in order to achieve the desired high-quality coating.

1.4 Research Objectives

The properties of PEO coatings, including high wear and corrosion resistance, high hardness, excellent adhesion and more importantly, a superior thermal barrier, suggest that the use of PEO coated pistons has the potential to improve ICE efficiency. The objective is to determine the impact PEO coatings on stock Al alloy pistons has on combustion in an SI ICE, to improve the efficiency and to meet evolving industry targets of reduced carbon emissions/fuel consumption. To address this objective, this study specifically compares the combustion in a standard engine setup with stock Al alloy pistons vs PEO coated Al alloy pistons by

- i) analyzing the combustion cycles at speeds and loads selected from a bsfc map overlaid with a drive cycle to determine the areas required for improvement

- ii) completing spark timing sweeps to analyze the effects across different combustion conditions
- iii) completing spark timing sweeps at different VCT angles to analyze combustion differences when small amounts of internal EGR are introduced
- iv) verifying that the full load peak torque and power conditions are undisturbed.

In this thesis, context is first provided with an in-depth review of coating types and coating process methods in development or in current use, in order to compare and contrast the potential advantages, and limitations of PEO coating in varied applications. Second, the method of the piston surface coating process will be detailed, with additional focus on the potential efficiency benefits of PEO coatings [20], specifically perusing the strong thermal properties. The engine setup and instrumentation required for analysis of combustion, with a full breakdown of the dynamometer cell setup and data acquisition system will then be described. The testing results will subsequently be reported, followed by discussion of the experimental findings. Finally, strengths and limitations of the project, and future directions will additionally be delineated.

CHAPTER 2 LITERATURE REVIEW

2.1 Literature Review Objectives and Overview

This literature review will present and discuss the various types of plasma electrolytic deposition (PED) coatings, including PEO, other production level coatings and future research prototype components for the automotive market. Also, other coating processes such as anodization, will be discussed so as to highlight the potential benefits of PEO coatings. The broad range of application for coatings across industries beyond automotive, including aerospace and biomedical, will also be addressed with the focus on PEO coating. The topics discussed and studies referenced in this section were compiled to inform the design and analysis of this thesis project, looking to build upon work that has already been completed in the field.

2.2 Coating Methods

There are many different types of coating methods that use techniques or application processes similar to PEO. Many of these coating processes have been brought to a production level of application such as, for example, Plasma Transferred Wire Arc (PTWA) Thermal Spray, which is a Ford Motor Company method [21]. Two very important objectives for the automotive industry are the reduction of fuel consumption and emissions. Fuel consumption can be decreased by reducing friction and the overall engine weight, and coatings can achieve both. With the reduction of engine weight being a necessity, the transportation industry switched to a hypoeutectic aluminum based alloy (AlSi alloys) engine block. However, the alloy requires protection from the high combustion temperatures. The common practice until recently was to use steel liners which are heavy, can be costly and if improperly machined or cooled, deform within the engine block. Coating applications to the bores of the block are now commonly used instead, and by replacing the steel liner, engine weight drops significantly. Examples of additional coating methods include RotaPlasma, developed by Sulzer Metco. It is a rotating powder fed atmospheric plasma spray system that has been used by Volkswagen. A rotating Twin Wire Arc (RTWA) system was developed by Daimler AG, which is in production with AMG. General Motors developed the High Velocity Oxygen Fuel (HVOF) system which uses a wire feed stock. The Ford Motor Company, as noted above, uses the PTWA developed by Flame-Spray Industries.

The following paragraphs review the details of the PEO-coating process, addressing advantages and limitations compared to other coating and coating methods. Given a Ford engine is used in this thesis project, it is of particular interest to first compare and contrast the PTWA and PEO-coating methods to appreciate the potential advantages of selecting the PEO-coated pistons for study.

In the PTWA coating process the plasma generator consists of a tungsten cathode, with an air cooled pilot nozzle made of copper, where the electrically conductive consumable wire is the anode [21]. The head, which is the component the nozzle is mounted to, is affixed to a rotating spindle. Similar to the PEO coating system used here, the head can rotate up to 600rpm. The wire is fed perpendicularly to the center orifice of the nozzle while the plasma gas is introduced through tangential boreholes situated in the cathode holder to ensure a vortex is created. The process begins with a high voltage discharge, ionizing and dissociating the gas mixture between the cathode and the nozzle. This allows the plasma to exit the nozzle at supersonic velocity where plasma is maintained from the cathode to the wire with an arc voltage of 100-120 V at a current of 60-100 amps. The gases used are a mixture of argon, hydrogen and compressed air to atomize and accelerate the molten particles. This culminates in high spray particle speeds of 100-130 m/s resulting in dense coatings with a low porosity. The thickness of the PTWA coating is roughly 200-300 μm , which is then machined down to a finished coating of 100-150 μm , slightly thicker than the PEO coating.

The requirement for machining to adjust PTWA coating thickness is a disadvantage when compared to PEO coatings, which require minimal material removal (roughly 10 to 20 μm), during post-deposition machining. Additionally, pre-treatment of the substrate surface is required with PTWA coatings to obtain a high bond strength that does not degrade over time. The Ford Motor Company uses the Ni/Al-Flux process to prepare the substrate surface for PTWA, but other forms of surface pre-treatment include grit blasting or high pressure water jet blasting [22]. PEO coatings in contrast, require very little pre-treatment (discussed further below). Both PEO and PTWA coatings however, are slightly porous surfaces which are able to hold very small amounts of oil, thus improving the oil storage capacity and the frictional behavior of the surface. PTWA coatings have been reported to produce a 6.8% reduction in friction on the cylinder bores of an engine compared to gray cast iron liners [21].

PED was one of the original terminologies applied to coating surfaces, and is defined as the process of spark or arc plasma micro-discharges in aqueous solutions that are utilized to ionize gaseous media from the solution to induce the synthesis of complex compounds on the surface of metals through the plasma chemical interactions. PED technology encompasses Plasma Electrolytic Saturation (PES) such as Plasma Electrolytic Nitriding/Carburizing (PEN/PEC), and PEO [12], which is also referred to as micro-arc oxidation (MAO), anodic spark deposition (ASD), plasma chemical oxidation (PCO) or anodic oxidation by spark discharge (ANOF) [13].

Originally, PEO was developed for coating metals other than aluminum, such as iron-based metals or copper surfaces. The results however were undesirable, with the iron-based metals exhibiting poor passivation behavior, and the presence of copper alloys in the substrate composition negatively affected the conversion process of the substrate [23]. PEO coatings on Mg and Ti materials exhibit lower mechanical stability than those produced on aluminum. For PEO coatings on aluminum, it is common to use silicate components which lead to large amounts of silicon oxides or alumina-silica-mixed-phases which generally increases the achievable coating thickness resulting in a compact morphology of the coatings. If there are excessive alloying elements such as Zn, Cu or Mg in an aluminum alloy, they can impede the transition from the metastable γ -phase to the high-temperature α -phase [24]. Depending on the target coating properties this can be a desirable transition.

All PED coating, (PEN/PEC, PEO), but predominantly PEO, provide a significant strengthening effect on aluminum substrates, resist significant external heat flux with lesser adhesion damage and offer dielectric properties. The high heat resistance is due, in part, to the higher porosity of some coatings, whereas the high electrical resistance can be a result of the high breakdown strength of silica and alumina. The cumulative effect is that PEO coatings display similar to superior benefits when compared to anodizing and thermal oxidation techniques, as well as providing an inexpensive low-weight alternative for materials in manufacturing and processing [12].

There are a multitude of different electrolyte solution groups for PEO coating processes that each promote different growth behaviors of the oxides resulting in varied beneficial properties. Different solution groups include: (1) solutions of salts that provide fast dissolution of aluminum, (2) electrolytes that provide slow metal dissolution, (3) electrolytes that provide metal passivation in a close range of voltages, (4) fluoride electrolytes which are characterized by complex behavior,

(5) electrolytes promoting slight passivation of the metal and (6) electrolytes that promote strong metal passivation. Solution groups 4-6 can be further divided into the following subgroups - solutions incorporating only oxygen into the coating, electrolytes containing anionic components or electrolytes containing cationic components, both of which enable incorporation of other elements into the coating, and suspensions providing cataphoretic transport of macroparticles contributing to the coating composition [12, 13]. Although these different solution groupings produce oxides of different compositions, all generate the same layer formation, or region division, when coating aluminum. There are three predominant regions - a porous outer region consisting of low temperature and X-ray amorphous phases, a dense inner region that is formed by high temperature modification and a thin interfacial region with complex phases of the substrate where alloying elements are observed [25, 26]. An example of the impact of different electrolyte composition and resultant coating properties is observed with increased silicate concentrate, which accelerates coating growth. This is due to the formation of complex Al-Si-O phases with the incorporation of Si into the coating structure [12].

PEO coatings can be described by three simultaneous processes - the electrochemical reactions, the plasma chemical reactions and the thermal oxygen diffusion [27, 28, 29]. During the process of coating, the electrolysis of aqueous solutions is accompanied by the liberation of gaseous oxygen or hydrogen [12]. The liberation of oxygen or metal oxidation occurs on the anodic surface (the substrate metal), while the liberation of hydrogen and/or cation reduction can also occur on the cathodic surface. The electrode processes are usually represented by a two-phase system with a single-phase boundary consisting of a double-charged layer in a more simplified model of the electrode-electrolyte interface. Typically, the cathode current density is higher than the anodic thus resulting in a faster cathodic reaction than anodic which is due to higher mobility of hydrogen ions through the oxide compared to ions containing oxygen [7].

AC or DC voltage can be used in the process of PEO applications. During the coating process it is important to choose the electric regime carefully, as whether direct, alternating, pulse current or voltage is used can drastically affect the quality of the coating [13]. For example, direct current or voltage discharge event continuously increasing can cause large discharge events over long periods which can deteriorate both the coating and the substrate. Therefore, it is most common to use alternating or pulse current or voltage to facilitate thick oxide coatings.

PEO coating provides the most cost-effective and environmentally friendly way to form a thick, ultra-hard and adherent ceramic oxide coating by the use of plasma discharges of light weight metals (Mg, Al, Ti) and their alloys [30]. The discharges, which can be modified, can have massive effects on the coating microstructure, thickness, roughness, porosity, hardness, coating growth rate and influence the phase transformations, crystallization and sintering. As previously noted, different current modes (AC, DC, unipolar, bipolar or hybrid) greatly affect the discharge density, local melting and oxidation of the substrate, and the quenching and re-crystallization process.

During the coating process the formation of the ion-conductive layer results in a significant electrical resistance that continues to increase as the layer thickens, therefore increasing electrical field strength is required for further current flow and coating growth [13]. Injection of the electrons at the electrolyte/gas interface acts as a quasi-cathode (equipotential area of the electric field) and a discharge channel evolves, penetrating the oxide layer. This results in thermally activated ions originating in the substrate metal, which are ejected out and away from the substrate because of the migration of the electric field and allows oxygen to move towards the substrate. This results in temperatures rising to several thousand Kelvin with the breakdown concentrated on the surface regions with the highest electric fields at the beginning of the coating process. During the evolution of the coating process the discharges become larger with fewer breakdowns evident. This can lead to issues that need to be addressed or observed with adjustments made to mitigate them. For example, the formation of high-temperature crystalline phases in the direct vicinity of discharge channels, can be heated, resulting in the re-melting of the oxide and large discharges, which can destroy the formed oxide layer [31]. Regardless, the PEO coating process has a very good throwing power resulting in a homogeneous coating in both thickness and distribution.

During the coating process local high temperature and strong electric fields result in molten oxide being ejected from the coating and substrate interface into the coating surface where it rapidly solidifies and is re-crystallized by the electrolyte [27]. This causes the fusing of the oxide and substrate material in the high electric field through discharge channels that are formed. The result is the coating grows outwards, to form the coating surface, and inwards towards the alloy substrate simultaneously [32]. Increasing the current density or voltage leads to an increased layer thickness and larger surface crater, where the changes in the current mode modifies the breakdown voltage and discharge events [33, 34]. Therefore, control or reduction of the strong discharges are required

to have a positive effect of the plasma temperature profiles, which lead to a denser inner layer microstructure with less porosity using a bipolar current mode [25]. Choosing a unipolar current mode would produce a thicker more porous coating with a higher surface roughness. Regardless of the method chosen the coating thickness increases linearly with coating time [17]. The large adjustability of the coating process, different alloying elements, and electrolytes means each coating has different phase compositions and surface morphology. The electrolyte concentration affects the breakdown voltage, the coating thickness, surface morphology, coating microstructure, porosity level and phase composition of the coatings, where the greater the concentration the lower the breakdown voltage and the thicker the coating [27].

When coating a substrate, shorting living micro-discharges are visible as plasma sparks across the anode or the substrate being coated [19]. This promotes the growth of the oxide layer on the surface of the object to be coated. When coating aluminum, migration of O_2^-/OH^- ions from the electrolyte to the aluminum anode occurs and Al^{3+} across the oxide during the electrochemical process. The hardness associated with PEO coatings depend on the amount of the Al_2O_3 crystalline phase. The morphology and the phase composition of the PEO coating are strongly influenced by the breakdown phenomenon. During the coating process of aluminum three types of plasma can be identified, the first being a strong plasma from the oxide film dielectric breakdown under the strong electric field. The second type of plasma occurs inside the surface or micro pores located fairly deep in the oxide layer. The third is the weakest plasma, occurring at the interface of the oxide coating and the electrolyte, or in the gas attached to this interface which is close to the very small holes in the oxide coating [19]. For the coating process on aluminum, the average diameter of the discharge channels is roughly similar to the thickness of the oxide.

During the coating process in the anodization phase the total current density is the sum of the ionic current density and the electron current density. Further in the coating stages, low voltage increases are required to maintain the same total current density. The flaws or defects such as fissures and micropores assist with the breakdown; the breakdown voltage is lower for degreased substrates and higher for electropolished substrates. After the initial breakdown an increasing number of micro-discharges are observed. Production of γ -alumina occurs because of local heating in PEO channels and direct crystal growth at the bottom of these channels, from the interaction of plasma and melted Al [19].

The electric breakdown during coating, results in a plasma state with anodic polarization resulting in a passive film being formed. The film is composed of oxides or hydroxides of the anode material with complex compounds of the substrate material along with the electrolyte components [13, 35].

The AC-pulse coating method begins with a passive film dissolving, which corresponds to the corrosion potential of the material. Then during re-passivation, a porous oxide film grows and at this time the majority of the voltage drop occurs. The electric field strength in the oxide film then reaches a critical value beyond which the film is broken through due to tunnelling ionization, at which point small luminescent sparks are observed to move rapidly across the surface of the oxide film supporting continued growth. Thermal ionization processes and slower, larger arc discharges subsequently arise. Thermal ionization is partially blocked by negative charge build-up of the thickening oxide film. Lastly micro-arcing occurs, and the film is gradually fused and alloyed with elements contained in the electrolyte. These micro-arcs penetrate through to the substrate.

In coating, after a certain voltage is surpassed, which varies based on the coating material and electrolyte composition [18], a drop of the anodic voltage takes place and transitions to the soft sparking part of the coating process. The soft sparking relates to highly developed participates on the surface and only starts after the whole surface is covered in these participates. The oxide layer surface is rougher and much more developed after the soft sparking transition. This also corresponds with the theory that the oxide layer must have sufficient thickness to change micro-discharge regimes and with a higher cathodic current the transition to the soft sparking can occur sooner. Lastly when the soft sparking transition is initiated, this is a good time to modify electrical parameters such as, frequency, duty cycles or overall current densities without losing this effect as long as the cathodic charge exceeds the anodic in every step [7]. This is a brief explanation of the PEO coating process for AC electric regimes.

There are important factors to consider that can affect the production of localized discharges in the area adjacent to the electrode during coating. Non-uniform distribution of the electric field in the vicinity of the electrode and the presence of dielectric film on the substrates surface. This can result in more intense arcing observed on sharp edges of the object being coated in both the PEO or PES coating processes. With the PEO coating process, the formation of a passivating (oxide) film promotes arcing over the whole surface which results in what is known as the bubble boiling conditions. Bubble boiling conditions occur with an AC-pulsed electric regime; use of a DC-pulsed

electric regime allows better control over the interruption of the coating process and therefore the arc duration can be modified along with the pulse form [12]. The principal parameter that needs to be controlled, regardless of the electrical regime and coating method chosen is the current density [36].

The pulsed DC electric regime [15], allows for more control of the creation of desired coatings compositions based on the electrolyte solution used and metal coated upon, such as thermal protection, wear or corrosion resistance. The Al, Mg or Ti alloy is always the anode and the stainless-steel electrode always the cathode with voltage starting low and gradually being increased over time. There is much variability with coating voltages and frequencies for the DC and pulse coating method. With different behaviors comes different temperatures; the average temperature ranges from 4500 K to 10000 K, but the base line temperatures of about 5000 K is similar for all frequencies. When coating, if peaks are required, the temperatures are measured to roughly 8000 K.

The coatings can have a high sintering effect with some porosity and holes within the coating near the oxide-metal interface. The surface morphology and cross-sectional microstructure are linked to the plasma discharge behavior. There is a possibility of gas escaping or getting trapped in the interface zone, where a longer discharge would result in better sintering and a denser coating. The discharge behavior heavily influences the microstructure and morphology of the oxide [15].

Summarizing, it is apparent many years of research have been completed assessing PEO coatings as alternatives for more expensive and heavy materials. The thermal properties, corrosion, hardness, lightness and low cost benefits collectively enable the application of PEO coatings to a broad range of uses. The tremendous customization and adaptability of the coating provides full control of the properties desired for the intended application. Thus, PEO coatings on the piston surface is a viable potential solution to improve ICE efficiency and meet the future targets set by the EPA.

2.3 Coating Applications

There have been many applications with the different coating and coating methods used in the automotive industry. Development of a new Nissan DI engine determined that the application of a mirror bore coating with a 0.2 mm thickness not only reduced engine weight significantly by

removing the need for heavy steel sleeves, but also reduced friction and natural vibration harmonics (NVH). The mirror bore coating reduced the friction on the surface of the bore by assisting oil retention, compared to a steel or cast-iron liner. This coating however required extensive after-treatment; aggressive machining of the coating was required to provide the mirrored finish [37]. Similar results were observed with the application of Mercedes's version of the coating, known as TWAS-coated cylinder liners or Nanoslide, which was applied to the cylinder bore of a turbo charged engine. The reduction of weight, friction and increased oil retention volume were also observed for the TWAS coating, in addition to favorable heat transfer properties, good fracture elongation and high heat resistance [38].

PEO coatings perform well as a thermal barrier, having very low thermal conductivity which helps in reducing the amount of heat transferred from the combustion cycle to combustion chamber components. In essence, the coatings serve as an insulating layer, increasing the heat energy available for conversion to mechanical energy. S. Özer and colleagues demonstrated PEO coating of engine components resulted in superior performance characteristics of various biodiesel/diesel/alcohol fuel blends [39]. Pistons and valves were coated on a single cylinder air-cooled diesel engine using an atmospheric plasma spray method to achieve a coating thickness of 100 μm . The coating powders used were a mixture of (NiCr) Al_2O_3 and 13TiO_2 (88% ZrO_2 , 4% MgO and 8% Al_2O_3). The coating produced was analyzed and showed $\alpha\text{-Al}_2\text{O}_3$ and $\gamma\text{-Al}_2\text{O}_3$ compounds with good homogeneously distributed elements.

The PEO-coated engine showed improvements in combustion efficiency leading to increased end of combustion temperatures, increased thermal efficiency, decreased bsfc and decreased CO emissions. The torque and power values also increased with the coated engine. A combination of O_2 content in the fusel oil with the coated engine reduces hydrocarbon emissions. The experiments consisted of full load testing at maximum torque and power engine speeds, evaluating the HRR using the first law of thermodynamics while neglecting wall heat loss. The improvements were related to the improved cylinder pressure values of 3-5%, suggesting the coated engine better isolated the heat, resulting in better efficiency. With the increased combustion temperature providing a good start to combustion, higher HRR was observed. These results were consistent across all different fuel types tested, even with the lower LHV, density and viscosity of the fusel

combined fuels. A negative outcome observed was the increased NO_x as a result of the higher combustion temperatures and pressures [39].

Of interest, the plasma spray method used in the Özer study can cause high porosity which can affect the thermal conductivity. The investigators reported the porosity of the coating to be low and there was a strong bond because of the indented, protruding and cavity free coating surface. This finding is not in keeping with the reported literature and the results here, in that typically, the higher the porosity the lower the thermal conductivity. Özer's work suggests that, despite the lack of porosity, PEO coatings maintain superior thermal conductivities.

Further studies have been completed on more modern engine designs, such as the Ford Puma diesel engine, again successfully employing PEO as a thermal barrier coating for reduced heat loss, thereby extracting more work from combustion during the expansion stroke [3]. With the reduction of heat transfer and increase of working heat energy the exhaust gases also increase, allowing for more energy recovery. This could be beneficial with the use of electric turbo compounding, thermoelectric generators or faster catalytic converter light off, improving cold start emissions [40, 41]. A current commonly used thermal barrier coating in production is the Yttria Stabilized Zirconia (YSZ), providing the best performance in high temperature zones of several traditional ceramic coatings. These coatings, however, retain the surface heat resulting in high temperature levels during the intake and compression stroke because of their large heat capacity. This results in volumetric efficiency decreasing along with working gas temperature increasing causing lower work output, higher emissions, and potentially higher knocking tendencies [42, 43, 44].

Recently, the Toyota Silica Rein Forced Porous Anodized Aluminum (SiRPA) coating using a process referred to as Thermo-Swing Wall Insulation Technology (TSWIN) was developed [45, 46]. The coating material has the capacity to rapidly change the wall temperature in a more dynamic way, following the transient gas temperature due to the low thermal conductivity and a low heat capacity nature of the coating. However, the SiRPA coatings have high roughness, negatively impacting performance by slowing combustion and increasing THC emissions [47]. PEO coatings provide benefits similar to these coating types, but with fewer drawbacks.

Hegab and colleagues evaluated the impact of two different methods of PEO coating, and a traditional anodized coating method, on pistons compared to a reference stock piston [3]. The PEO

coatings, using a Keronite method, were comprised of a mixture of α -alumina and γ -alumina with silicate phases such as mullite, at a thickness of 65-75 μm , with a uniform coating and pore structure across the surface [48]. The incorporation of mullite, an aluminosilicate, together with a high porosity, gave these oxides very low thermal conductivities of the order 0.45-0.8 W/mK [48]. The high porosity, while not hindering the durability or surface roughness, assisted with the low thermal conductivity as air has a low thermal conductivity and high heat capacity [49]. Multiple engine speeds and loads were run with injection timing sweeps performed at each set point to analyze the trends for each piston. The PEO-coated pistons demonstrated higher cylinder pressure and higher cumulative heat release while having better fuel conservation compared to the anodized and stock pistons. This was attributed to the increased insulating effect of the PEO coating due to its highly beneficial thermal properties. There is less heat transfer increasing the in-cylinder temperature. This results in shorter ignition delay and an earlier start of combustion, increasing the cylinder pressure [50]. Comparison between the stock pistons and PEO-coated pistons showed a 3% increase in the cumulative heat release as a result of the reduced heat loss increasing the work per cycle on the piston. The shift and increased temperatures allowed more work to be extracted during the expansion phase resulting in reduced exhaust gas losses. Reduced heat transfer and increased in-cylinder temperatures with closer to TDC combustion improved the soot emissions as it promotes oxidation of soot in the flame zone. This also leads to reduced THC emissions with the best result observed on the smoothest surface PEO-coated piston, with the lowest porosity. The smooth surface and low porosity prevent unburnt hydrocarbons from being trapped in the coating porosities. CO emissions were found to be comparable to the uncoated piston, despite the more desirable elevated temperatures for the oxidation process. The second PEO-coated piston with a higher porosity had higher CO and THC emissions, because the unburnt fuel/air mixtures get trapped in the porosities. A negative effect observed was increased NO_x output regardless of the PEO-coated piston, with the peak being at the most advanced injection timing. NO_x formation occurs under high in-cylinder temperature and peak cylinder pressure conditions. Despite the higher NO_x output the result of this study found under ideal part load conditions, a 3% increase in the thermal efficiency as a result of the reduced heat losses [3].

Further applications for PEO coatings involve environments that require quick moving parts in aggressive atmospheres. PEO coatings are ideal for these conditions because of their superior wear and corrosion resistance along with their low overall density [13]. PEO coatings are also of

interest in aerospace engineering applications because of their excellent thermocycling resistance due to good substrate binding. This allows massive temperature fluctuations without flaking of the PEO layers. Coating with PEO additionally provides corrosion protection and reduces contamination due to the low outgassing tendencies, which is highly relevant to reducing degradation of optical devices. The coatings have been observed to have a good solar absorbance which is beneficial for passive thermal control in space or vacuums. The unique coating methods of PEO allow the coating to permeate areas of limited accessibility in complex designs, allowing inner walls of heat sinks to be coated, for example [13].

PEO coatings have also been utilized in the medical engineering industry due to their properties of non-toxicity, biocompatibility, chemical stability and minimal corrosion tendencies. Since titanium and PEO coatings are not bioactive there is no chemical bonding between bones and the implants, which is highly beneficial for temporary implants. For permanent implants, when bioactivity is required for bonding, PEO coatings can be modified to assist in the production of a bioactive surface such as hydroxyapatite coatings [13]. Lastly, PEO coatings have proven useful in dental applications using the coating on the locaters which are placed on impressions of oral cavities to help reduce the optical reflection of the laser light, generating higher quality data.

The applications described in this section, from an automotive perspective, consider the two main fundamentals of the PEO coatings: 1) the reduced friction capacity and 2) the reduced heat transfer or thermal conductivities. Both properties improve the ICE efficiency. The current literature supports the use of PEO-coated pistons in the present study. The specific target of this project is to reduce the heat transfer and increase the cylinder pressure, HRR, bulk gas temperatures, and exhaust temperatures with the use of PEO-coated pistons.

CHAPTER 3 EXPERIMENTAL DETAILS

3.1 Engine Setup

The engine chosen for this testing was a 7.3L Ford engine which is designed for the F350 to F550 fleet vehicles or commercial trucks. The Ford engine is a 90°V push rod in block cam or Overhead Valve (OHV) engine with a Dual Equal VCT; engine specifications are detailed in Table 3.1. A Dual Equal VCT means the intake and exhaust, advance or retard, at the same rate because they are locked together and cannot be controlled individually. Therefore, the overlap between the exhaust valve closing and intake valve opening cannot be adjusted. The control range for the VCT timing is 50° retard. The engine cylinder head is a 2-valve design with a large intake valve and a smaller exhaust valve. The engine oil and filter used were standard spec, where the oil grade was 5W30 for this engine and was filled to the factory fill specifications. A stock engine powertrain control module (PCM) was used in addition to a standalone engine management hardware/software during the tests, to ensure the maximum possible efficiency could be achieved without potential limitations from parameters in a stock PCM software setup. After the preliminary testing, the stock PCM had shown limitations that impeded the assessment, therefore the remainder of the testing was conducted on the standalone management system.

This engine platform was chosen because fleet vehicles accumulate substantial idle time, but also run at, or close to full load during driving, the majority of the time. Passenger vehicles do not commonly experience these extreme conditions. The engine idle conditions are typically the least efficient running conditions and therefore it is an important and potentially rewarding area on which to focus to improve efficiency. The aim was to study the efficiency differences at idle conditions together with low load, low speed conditions while ensuring the engine delivers unchanged full load performance.

Table 3.1 – Engine specifications

7.3L Ford	V8
Volumetric Displacement	7.29 L
Volumetric Displacement Single Cylinder	0.000912 m ³
CR	10.5:1
Induction System	Naturally Aspirated
Cooling System	50/50 Glycol/Water
Bore	107.2 mm
Stroke	101 mm
Fuel System	Multi-Port Fuel Injection (PFI)
Valves per Cylinder	2
Valvetrain	Single Camshaft
Variable Cam Timing	Dual Equal

The engine was fully instrumented ([Figure 3.1](#)) with piezoelectric pressure transducers of type Kistler 6025C and referenced to TDC of cylinder #1 using a Kistler 4045A5 5 bar manifold absolute pressure (MAP) transducer, ([Appendix Figure A.30](#)), coupled with an AVL 365C crank angle encoder mounted to the crankshaft of the engine, ([Appendix Figure A.32](#)). Further detail of the sensor setup is discussed in the Combustion Analysis System (CAS) section ([Section 3.4](#)). Temperatures and pressures were measured from T1/P1 to T4/P4, with all pressures recoded via gauge pressure on the cell side data acquisition. Pre-airbox temperature and pressure, or barometric pressure, were measured together with ambient air temperature. A combustion air system was used to control desired intake air temperature and humidity. Further downstream in the airflow path at the intake manifold, the pressure and temperature were measured with the thermocouple and pressure sensor located in intake runner #1. Fuel flow was measured at the fuel cart and fuel pressure and temperature were measured as close as possible to the fuel rail. The fuel cart simulates a vehicle spec returnless fuel system and the fuel pressure was adjusted to meet spec fuel pressures for this engine. After the combustion chamber, exhaust gas temperature and pressure were measured downstream of the collector on both the right and left side of the exhaust system. The cell exhaust has fully separated left and right exhaust flow paths. The exhaust back pressure was set to spec vehicle backpressure, which normally results from the catalytic converter and muffler, via plates with different size orifices.

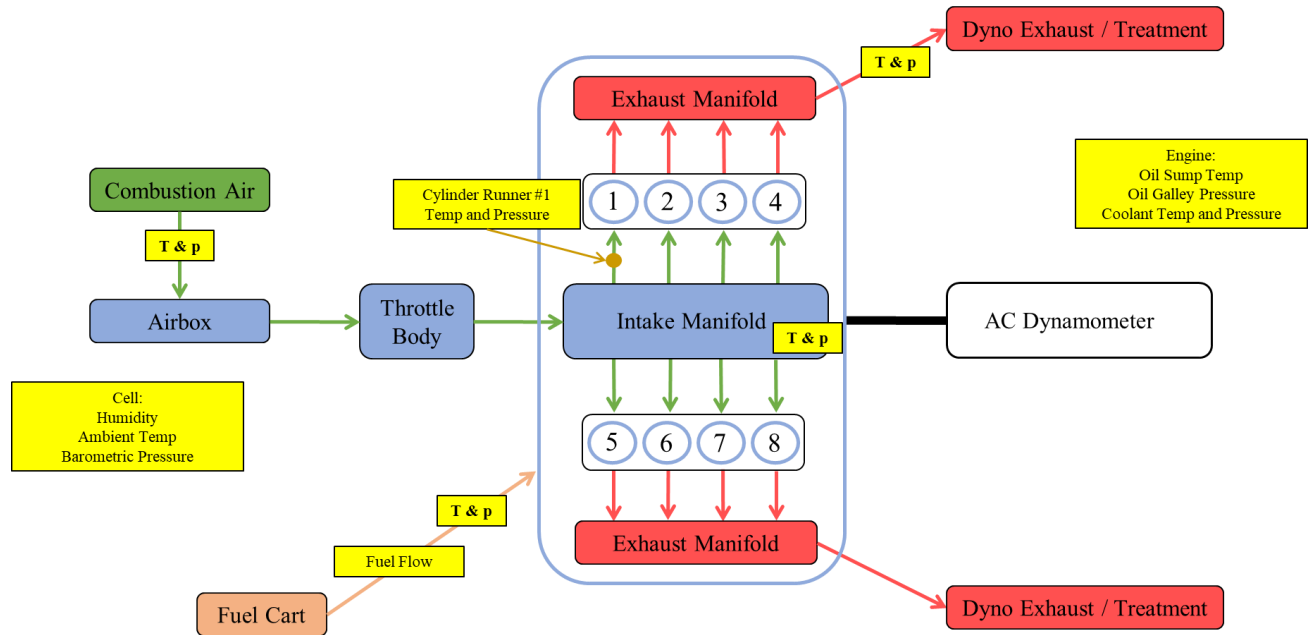


Figure 3.1 - Engine and dynamometer cell setup and instrumentation

The engine coolant temperature and pressure were both measured and controlled to meet standard vehicle operating conditions. The coolant out temperature was controlled via an independent heat exchanger with a PID controller operating a valve allowing the cooling water to pass through the heat exchanger when required. The coolant pressure was controlled via pressurized air feeding the cooling loop through a digitally controlled regulator with real-time feedback and control. Oil sump and galley temperature were measured. The oil sump temperature was controlled in the same manner as the engine coolant. The oil sump temperature did not require control at the lower speeds and loads as heat generated was insufficient to meet the setpoint. Instead, oil temperature was allowed to stabilize at the lower speeds and loads to ensure similar oil temperatures between the tests. Oil pressure was measured at the oil galley. The pressure and temperature control setpoints are listed in Table 3.2. Precise control of these boundary conditions were necessary to both keep the engine healthy and prevent damage, and to ensure reduced variability between runs as temperature and humidity have a large effect on combustion.

Table 3.2 - Engine temperature and pressure control parameters

Control Parameters	Set Points
Coolant Temperature	195 °F
Coolant Pressure	21 psi
Oil Temperature	265 °F (when required)
Fuel Pressure	55 psi
Intake Air Temperature	77 °F
Intake Air Humidity	0.6 - 0.7 gH ₂ O/kgAir

3.2 Process for Coating the Pistons

The PEO coating process used for this study was a pulsed DC voltage electric regime method with modifiable frequencies allowing changes to the voltage, frequency and wave shape of the amperage being applied. The DC pulsed method does not require extremely high constant voltages to assist with the breakdown of the dielectric barrier or the discharge of the electrolytes. Instead, the DC pulsed method uses a square wave frequency increasing and reducing the amperage supplied during the coating process to promote the dielectric breakdown of the electrolytes and the substrate surface. The voltage and amperage verses time is shown in Figure 3.2. This method is similar in principle to the AC pulse method where the AC current spikes are required to help with the discharge of the electrolytes, but the pulsed DC electric regime was chosen instead because of its superior control capabilities. The pulsed DC electric regime was configured to achieve high coating porosity without risking structural integrity, achieving a smooth low roughness finish, with a high coating density, high thickness and good homogeneity across the surface of the piston at a fast growth rate. These factors are all important to ensure the durability of the coating on the surface of the piston.

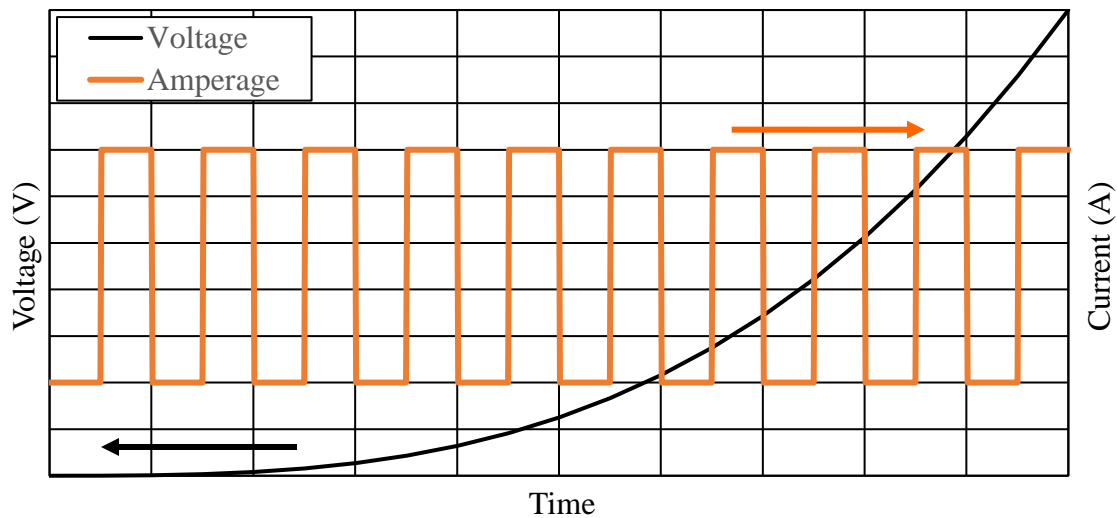


Figure 3.2 - Voltage and current versus time for the DC pulsed PEO coating method represented as an absolute

Prior to the initiation of the coating process a cover had to be designed to protect the parts of the piston that did not require coating including, for example, the skirts, rings area and the bottom. The purpose of this cover was to not only prevent coating of specific areas of the piston, but also to reduce the discharge area as shown in Figure 3.3. The stock piston is displayed in the left image and the composite protective cover for the PEO coating process displayed in the right image. As mentioned prior, the discharge generates substantial heat, so reducing the discharge area helps regulate this heat generation thereby decreasing the difficulty of ensuring a well adhered low roughness coating. The electrolyte solution was also cooled by an indirect heat exchanger system passing cooled water through the copper coils in the electrolyte holding tank.

After the cover was designed and test fitted to the piston, both the piston and cover are placed into the electrolyte solution tank, as shown in Figure 3.4. The piston, fitted with a protective cover, is submerged in the electrolyte solution tank and displayed in the left image; thus resulting in the desired restricted deposition of piston coating displayed in the right image. The piston was connected to the anode and a sacrificial stainless-steel bar was placed in the electrolyte solution to be connected to the cathode. The electrolyte assists with the discharge and, for this study, consisted of a 5-8 g/L sodium silicate containing a high silicate concentration because this results in excellent

thermal conductivity properties. Electrolytes with high silicate concentrations induce the deposition of large amounts of silicon oxides or alumina-silica-mixed-phases which, coupled with high porosity, uniform coating and pore structure, gave very low thermal conductivities.

Piston coating was performed at the Ford Motor Company by Guang Wang (PhD candidate University of Windsor). The coating process took about 30 minutes per piston with a final voltage of 500 V and the maximum of 40-50 amps at the peak of the square wave frequency. This coating process consumed roughly 8 kWh of energy per piston. The starting voltage began at roughly 100 V and then rises to the final value of 500V over the 30 minute period in a parabolic form, because as the thickness of the coating increases the electrical resistance increases. The dielectric breakdown occurs at a field of 10V per micron. The amperage oscillations via adjustments in the pulse frequency were adjusted and specifically set to produce the highest quality coating for this application based on the properties of the piston and electrolyte. All of these adjustable parameters resulted in the total energy consumption, to coat all eight pistons, of roughly 64 kWh costing roughly \$7.36 based on Enwin Utilities industrial electricity costs [51]. This was the base cost excluding delivery fees, taxes and based on the winter 2022 industrial cost of electricity in the Windsor, Ontario, Canada area for a business that uses more than 750 kWh.

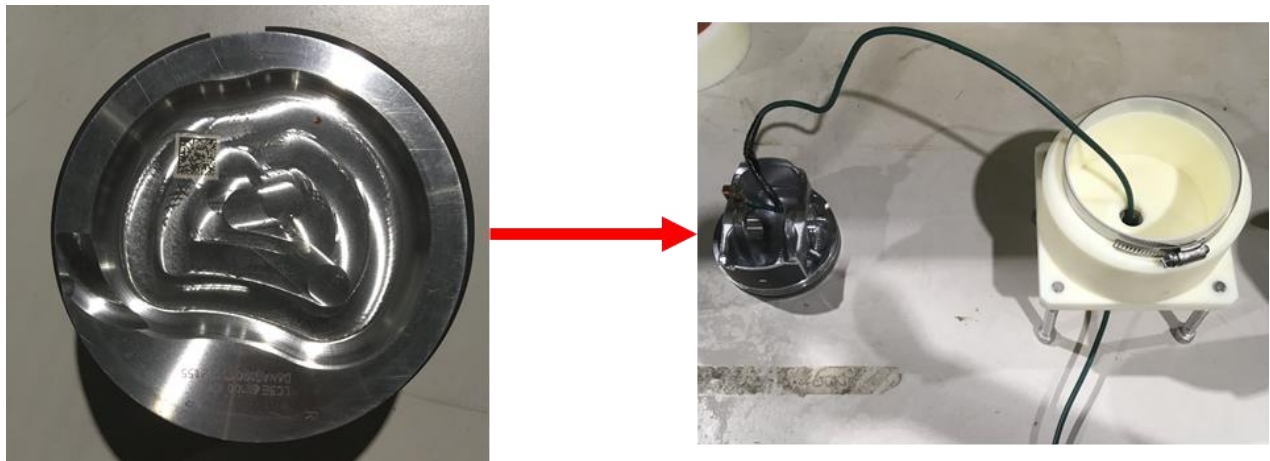


Figure 3.3 - Stock piston and cover for coating process

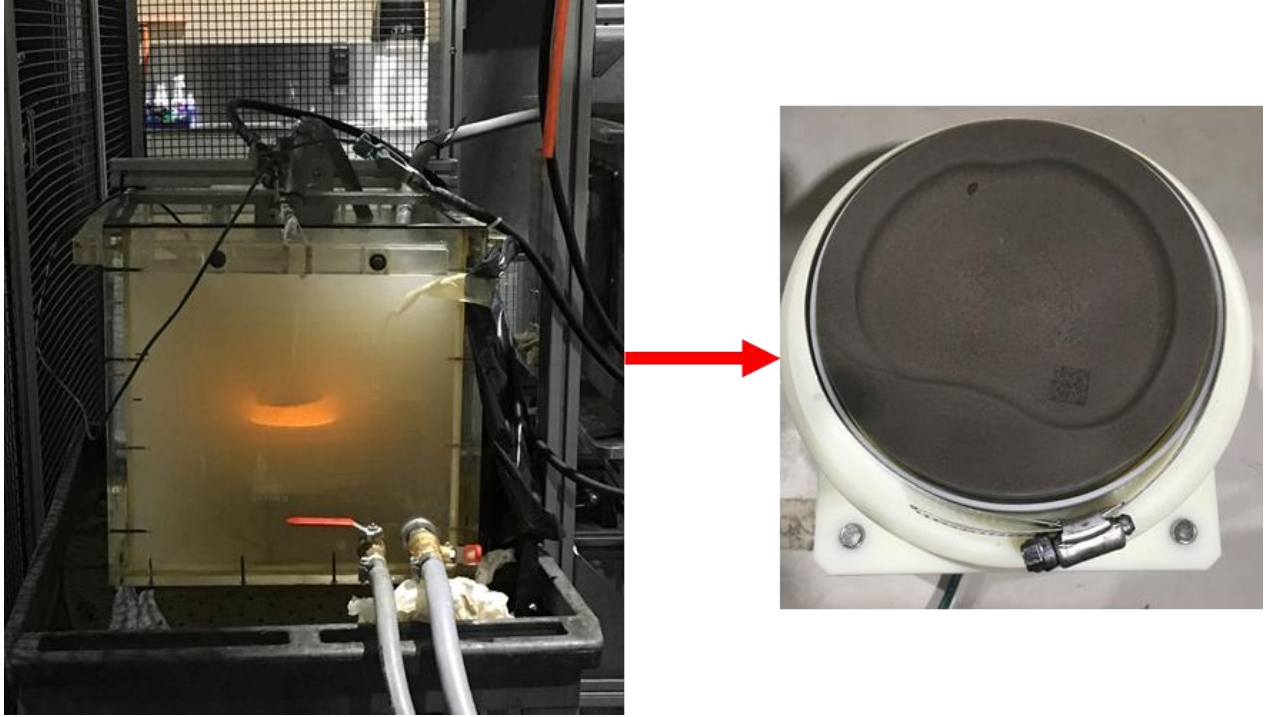


Figure 3.4 - Electrolyte solution tank during the coating process and coated piston.

After the coating process was complete the piston and cover were removed from the electrolyte solution tank and analyzed. The coating was an alumina coating consisting of a relatively dense polycrystalline layer of alpha-alumina, with a softer, more porous layer of gamma-alumina formed on top. The piston was cleaned, and the coating thickness was measured to be approximately 100 μm thick. Surface smoothing was completed by wet sanding to remove any burs or rough spots; no further machining was required. The roughness was measured to be approximately 1 μm using a profile meter. The porosity is related to the voltage and current settings and was high for the pistons as a high current profile was used resulting in a high discharge rate. The high porosity coupled with the high silicate oxide properties resulted in a very low thermal conductivity to the order of less than 1 W/mK. The coating had a homogenous and uniform consistency across the piston surface. The final finished product of the coated piston is shown in Figure 3.5. The piston surface or crown was PEO-coated with the compression rings and oil rings installed. This piston is now ready for installation into the engine.



Figure 3.5 - PEO coated piston finished product

3.3 Dynamometer Cell Setup

The dynamometer cell setup delineates all factors that must be considered for engine testing, including the sealed room, the dynamometer itself, the controllers and the acquisition systems. The dynamometer cell used for this study was not a climate-controlled cell and therefore airbox air-in temperature and humidity were controlled with a combustion air unit. The combustion air unit regulated the air temperature and humidity to a desired setpoint through the use of a heater, conditioner and a steam generator. The control feedback was acquired via a Vaisala unit which measures the temperature, barometric pressure, vapor pressure, and the relative humidity. Specific humidity was calculated from the barometric pressure, air temperature and dew point temperature. The air was directed to the airbox from the combustion air unit via ducting. The combustion air must be measured at the airbox inlet as the heat from the engine and humidity in the cell can affect or contaminate the air entering the airbox; a perfect seal was not possible. The barometric pressure and ambient temperature were recorded and monitored as well, since these could not be controlled inside the dynamometer cell.

The supplied fuel for the engine was controlled by a standalone unit or fuel cart that allows for fuel pressure and temperature setpoints to be adjusted while measuring the fuel flow. The fuel was

supplied to the fuel cart by a gravity fed system to ensure a constant supply of fuel flow and pressure. The fuel cart then increases the pressure to the required set point. Collectively this system best simulates the in-vehicle fuel supply system.

The dynamometer selected for use in this study was an AC Medien Dynamometer, (Appendix Figure A.31). The AC dynamometer is preferred for steady-state testing as it allows for more refined control of engine speeds and torques. The torque transducer selected for the dynamometer setup was a strain gauge load cell with a Wheatstone Bridge circuit design.

The controls system for the dynamometer set-up and operation consisted of multiple computers; one with software controlling the operating systems, one real-time computer as a communication translator and a PXI chassis for the hardware hub or systems backbone. The software computer controller system was on a standalone computer running Linux, using CAN and Ethernet communications for cross talk between the real-time computer and PXI chassis. The control parameters for adjusting and running the dynamometer cell are all centralized on the main control computer together with all data analysis logging. The powertrain control module (PCM) parameters were output to the main dynamometer cell systems computer at 20Hz and logged on the main dynamometer cell computer.

3.4 Combustion Analysis System (CAS) Setup

An A&D Phoenix AM/RT combustion analysis system (CAS) was used to capture the in-cylinder pressure data and reference it with respect to the crank angle and cylinder volume, (Appendix Figure A.30). The CAS system was used to capture cycle-by-cycle real-time (RT) data. Cylinder pressure transducers were required to capture this data and the ones selected for use are capable of up to 300 bar measurements, (Figure 3.6). The red arrows indicate the individual cylinder pressure transducer locations in the left image. Kistler cylinder pressure transducer can be seen in the right image. For this study, to increase resolution the pressure transducers were calibrated in the partial range of up to 200 bar. The peak firing pressure for this engine is below 100bar, but to ensure heavy knock or pre-ignition measurement capability a wide range of pressure needs to be available. All eight cylinders were instrumented to ensure cylinder-to-cylinder variability was accounted for, (Figure 3.6). The crank angle encoder used was set-up at a 0.2° crank angle resolution, to ensure possible knock events could be captured. The crank angle encoder's optical function is based on a

slot mark disk and utilizes the reflection light principle. The crank angle encoder was mounted to the crankshaft of the engine via a machined encoder hub that is mounted to the damper of the engine with the stock crank bolt. A 5 bar MAP Kistler sensor was installed in the intake runner of cylinder #1 to give the cleanest intake pressure pulses for pegging the pressure traces.

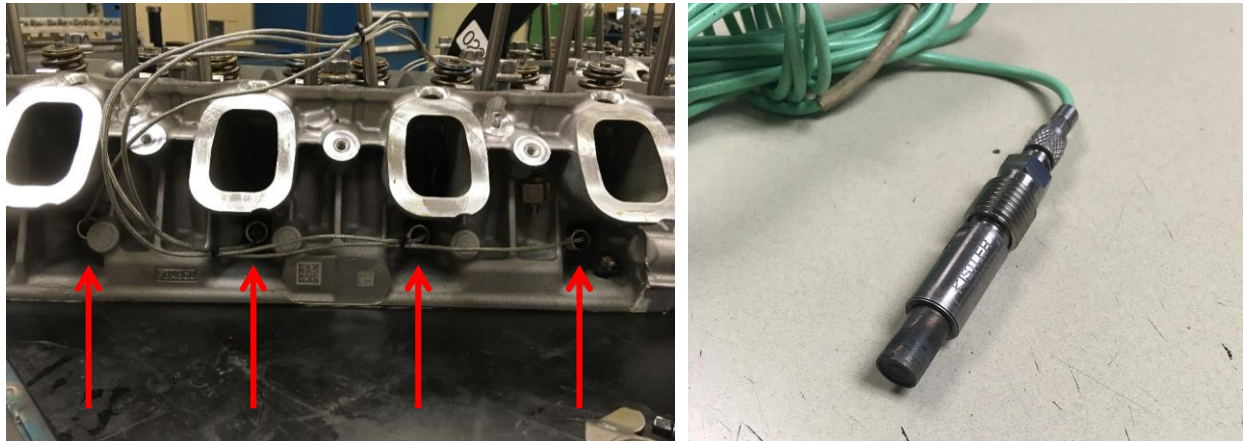


Figure 3.6 - Kistler cylinder pressure transducers and installation location

The electronic components, AVL encoder amplifier and light tube, cylinder pressure transducer charge amplifiers, were mounted separately from the engine to minimize any potential electrical, temperature or vibration interference. The high crank angle resolution was required for knock measurements which the CAS software calculates real-time. The CAS system calculates knock through the use of the cylinder pressure signals which are digitized prior to analysis. Once the raw cylinder pressure signal has been digitized CAS generates a smoothed pressure trace using an adaptive averaging window, or also known as a moving average filter. The original trace is then compared to the filtered trace generated over the knock window range, which was set from 0° to 60° ATDC. This generates a new trace, subtracting the filtered trace from the raw data, to give a trace that can be used to calculate knock parameters such as knock peak-to-peak and knock amplitude. Knock peak-to-peak is the amplitude of the pressure oscillations due to knock found on the filtered cylinder pressure signal. Knock amplitude is the maximum value achieved on the

rectified-filtered knock signal trace. An example of a raw cylinder pressure trace showing a knock event versus a normal no knocking combustion cycle can be seen in Figure 3.7.

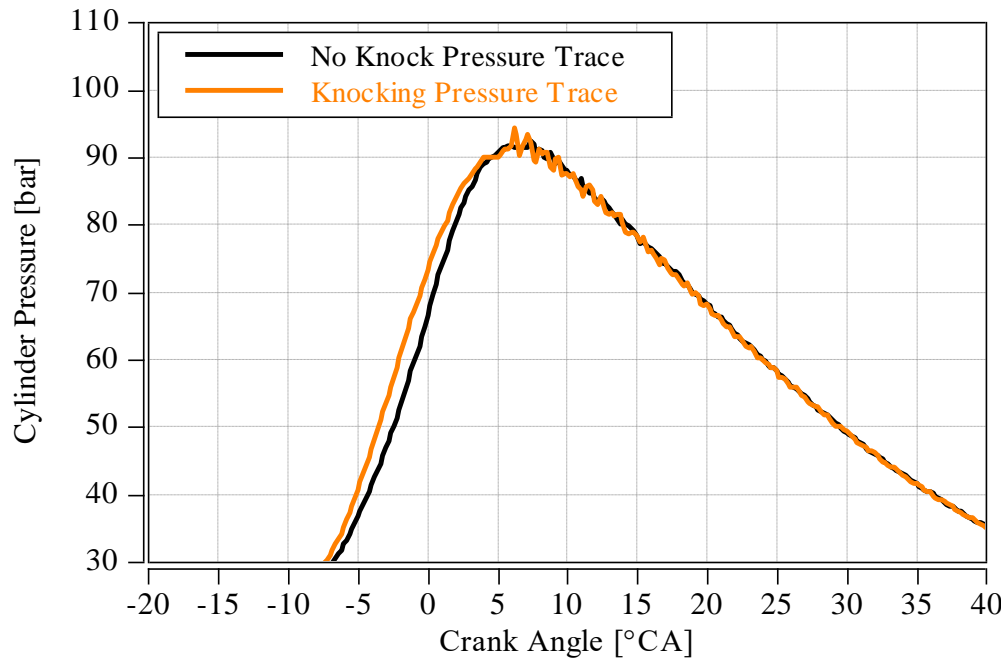


Figure 3.7 - Cylinder pressure traces showing knocking vs no knock combustion cycle events

The CAS data was taken over 300 engine cycles at the 0.2°CA giving 1800 points per combustion cycle. The unfiltered cylinder pressure traces were used to calculate the HRR, combustion duration, indicated mean effective pressure (IMEP) and pumping mean effective pressure (PMEP) among other parameters. Cylinder pressure traces were also used to calculate the standard deviations (STD) and coefficient of variation (COV) using averaging [52].

3.5 Test Setups

Testing was first completed on the stock engine to capture baseline data. The engine was then torn down and rebuilt with the PEO-coated pistons. The coated-piston height was measured and found to be no different from the stock piston height. Despite the growth of the coating both into and out from the substrate there was a net zero change in piston height. Therefore, there is no compression

ratio change that needs to be taken into account during testing or analysis. New compression rings and oil rings were installed with the coated pistons and thus a break-in and friction stabilization were performed to ensure proper seating of the rings. The engine was fully warm at standard operating temperatures for the coolant and oil temperature during all data collection.

Testing consisted of completing a Ford Motor Company standard mini-map point to establish a baseline difference between the two setups. A mini-map test and transient test cycle overlaid on a bsfc map from a representative standard setup, delineating the differences in fuel efficiency, is shown in Figure 3.8. Dark red represents better fuel economy and blue worse fuel economy and yellow points indication areas of interest to study. The equation for bsfc, shown below (Equation 1), is the measure of the fuel efficiency of the engine and represents the power-specific fuel consumption. The general standard units for bsfc are g/kWh. It is an important parameter to calculate as it permits direct comparison between engines. The bsfc map with the overlaid real world drive cycle was used in conjunction with data collected from real world applications of super-duty engine operations (eg. low load and full load condition) to select main points to analyze. Being that these engines are in work-horse trucks sold for commercial use, they accumulate many idle hours. Super-duty trucks will also tend to spend most of their driving time at full load high speed conditions because they are at, or near to, full capacity with large and/or heavy loads. Therefore, idle, low speed low load and full load high speed points were picked to observe and study the combustion differences between coated and uncoated pistons.

$$bsfc = \frac{\text{fuel mass flow rate}}{\text{brake power}} \quad (\text{Equation 1})$$

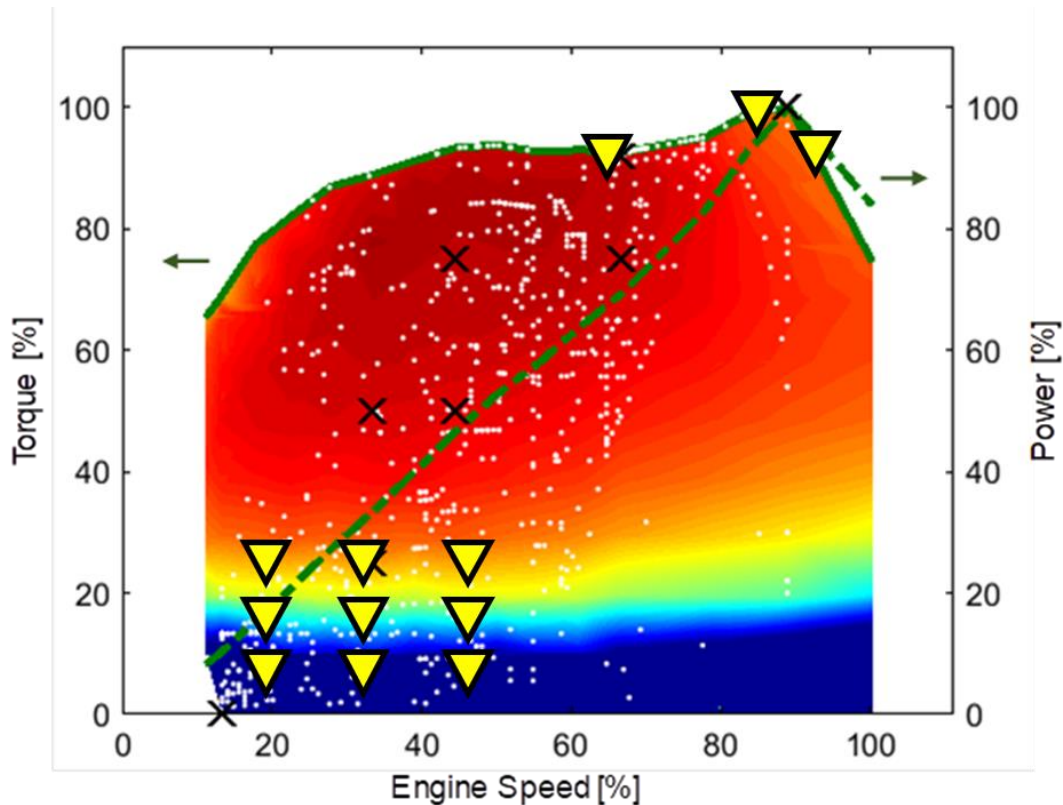


Figure 3.8 - Mini-map points and transient test cycle overlaid on a bsfc map

Once a baseline was established between the coated and uncoated pistons using the mini-map speed and load points, spark and VCT sweeps were performed. The spark and VCT sweeps were performed at various low speed, low load points across the full range of the VCT, 0-50° retard @ 5 deg increments, as shown in Table 3.3. During this testing both constant load and constant throttle runs were completed to observe possible increases in efficiency. The intent here was to study potential idle stability improvements, reduced COV IMEP and overall efficiency increases resulting from the PEO-coated pistons. Spark and VCT sweeps were also performed at high load, high engine speed points as shown in Table 3.4. Since these engines are required to perform for long periods of time under high stress conditions it was additionally important to ensure the coating did not compromise full load, high speed conditions. Knock was of particular interest as stock pistons typically dissipate substantial heat through them.

Table 3.3 – Selected low load spark sweep and VCT sweep points

Speed [rpm]	Load	VCT Set Points [deg]
1000	0.2, 0.3, 0.4	VCT Sweep 0 - 50 @ 5° Increments
1500	0.2, 0.3, 0.4	VCT Sweep 0 - 50 @ 5° Increments
2000	0.2, 0.3, 0.4	VCT Sweep 0 - 50 @ 5° Increments

Table 3.4 - Selected high load spark sweep and VCT sweep points

Speed [rpm]	Load	VCT Set Points [deg]
3000	Full Load	VCT Sweep 5 - 15 @ 5° Increments
3500	Full Load	VCT Sweep 5 - 15 @ 5° Increments
4000	Full Load	VCT Sweep 5 - 15 @ 5° Increments

Cell side data was taken at rate of 10Hz over a 30 second period giving 300 data points for each test set point, Figure 3.9. Standard deviation was calculated by averaging this data. At each test setpoint anywhere from 5 to 10 data sets were collected at each speed and load to give the data group. These data groups were then analyzed for trends across the spark and VCT sweeps to build a map potentially showing areas of improvement and areas of retrogression.

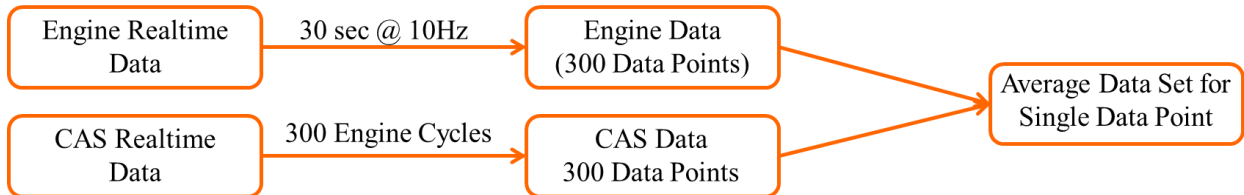


Figure 3.9 - Data collection flow diagram

3.6 Quality Checks

Quality checks are essential since a 1° misalignment of the TDC offset can drastically change the outcome of data acquisition. Quality checks were continuously performed on all data collected and processed to ensure data accuracy. TDC checks to ensure TDC offsets were correct, with no error in the encoder’s offset or reference to cylinder #1 in CAS, were performed daily. Figure 3.10 shows the cylinder volume versus crank angle or theta, showing the TDC and BDC for cylinder

#1 and confirming the absence of a TDC offset error. Post process pressure pegging checks were completed and shifted, when necessary, as CAS performs pressure pegging calculations real-time and offsets the pressure trace accordingly. Confirmation of data quality was performed on all processed data through the use of the Log p vs Log V graphs, Figure 3.11, by checking the polytropic coefficients of expansion and compression. The polytropic coefficient of expansion represented by the blue line and the polytropic coefficient of compression represented by the green line. The polytropic coefficients are calculated by curve fitting a line to the Log p vs Log V data at the point where the respective valves are closed during the compression/expansion stroke and calculating the slope of said line. Good quality cylinder pressure traces should result in targets of 1.3 to 1.35 for the polytropic compression coefficient and 1.3 for the expansion coefficient. Engine quality checks were also performed intermittently during testing to ensure the engine health had not changed altering the data.

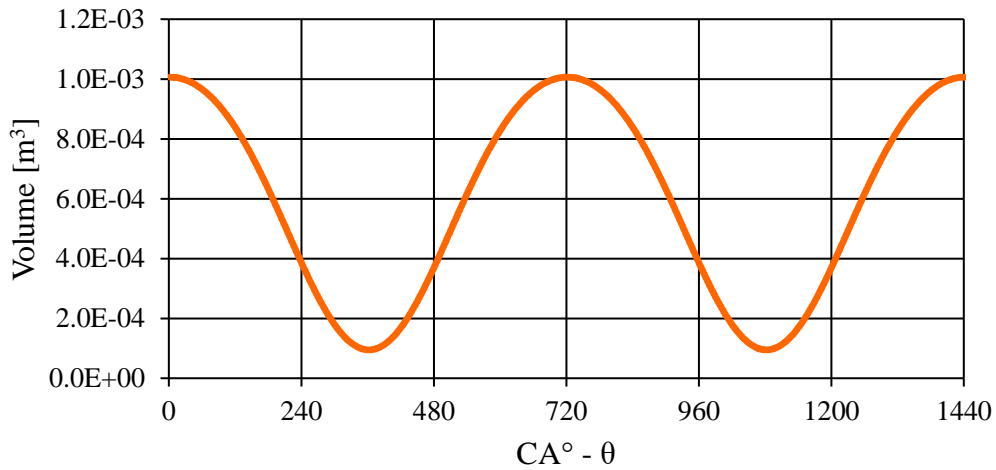


Figure 3.10 - Volume vs Theta graph

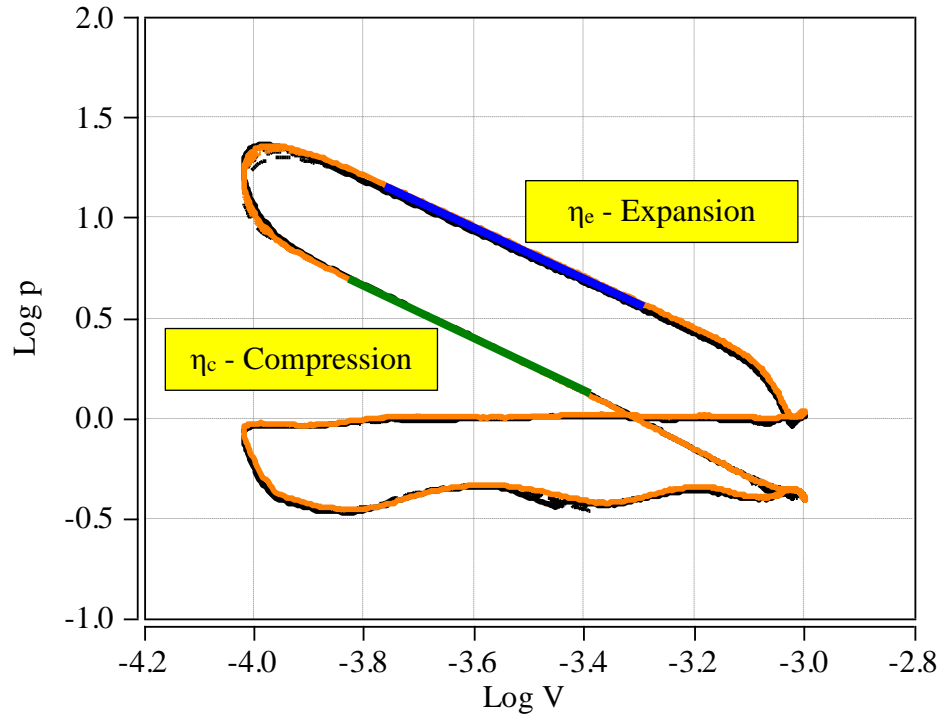


Figure 3.11 - Log p vs Log V graph for cylinder pressure data quality check

CHAPTER 4 EXPERIMENTAL RESULTS

4.1 Data Processing

Cylinder pressure data was collected at a 0.2° CA resolution and processed at this resolution for the knock data. For all other parameters the cylinder pressure data was down sampled to a 0.5° CA resolution for data processing. Pressure pegging, as mentioned earlier, was performed by the CAS software. However, secondary pressure pegging checks were completed and re-performed on the cylinder pressure traces if required. A quality check using Log p vs Log V was first performed; if η_c was found to be out of spec the pressure pegging check and a correction was performed using cylinder pressure versus crank angle data, seen in Equation 2 [53]. In the equation p_{peg} is the intake manifold pressure at the intake valve closing event captured using the MAP sensor located in intake runner #1 and the summation of the pressure data is taken over a 10° CA duration at the intake valve closing event.

$$\Delta p_{ref} = p_{peg} - \frac{1}{n+1} \sum_{\theta_{ref}-n/2}^{\theta_{ref}+n/2} p_{meas}(\theta) \quad (\text{Equation 2})$$

HRR is the rate at which chemical energy of the fuel is released by the combustion process. It is calculated from the cylinder pressure vs crank angle data. There are three more commonly used descriptions to characterize the energy-release zones of the SI combustion process – the flame-development angle, the rapid-burning angle and the overall burning angle. The flame-development angle is defined as the period after the spark when a small but significant fraction of the fuel energy has been released (CA10). The rapid-burning angle is defined as the duration between the end of the flame development stage and end of flame propagation (CA10 to CA90). The overall burning angle encompasses the period of the complete combustion process. The heat release model is based on the First Law of Thermodynamics with the following assumptions: 1) uniform thermodynamic properties and gas composition throughout the combustion chamber, 2) apparent heat release process based on the averaged properties in a single zone equilibrium thermo-chemistry and 3) the sensible enthalpy from the fuel injection is neglected [54]. From these assumptions the apparent

net heat-release rate equation can be derived (Equation 3) [53]. also assumes the contents of the cylinder are modeled as an ideal gas and the specific heat ratio (γ) is 1.33.

$$\frac{dQ_n}{d\theta} = \frac{1}{\gamma - 1} \left[\gamma p \frac{dV}{d\theta} + V \frac{dp}{d\theta} \right] \quad (\text{Equation 3})$$

The calculation of bulk gas temperature is a reasonable estimate of the PEO coating thermal barrier effects and can be calculated using the combustion chamber volume and cylinder pressure traces. Collectively considering the assumptions of the conservations of mass and energy and the ideal gas law (Equation 4), we can calculate the bulk gas temperatures. The cylinder pressure data was processed at a 0.5° CA resolution. We assume the temperature of the air-fuel charge to be equal to the intake runner temperature of cylinder #1, since this is a port fuel injection engine with closed valve injections. Therefore, assuming an adiabatic process, the unburned gas is initially uniform [54] and Boyle's Law of thermodynamics between each 0.5° CA pressure and volume increments, produces the bulk gas temperature Equation 6. Equation 6 is derived from Equation 5; the specific heats are constant because of the assumed adiabatic polytropic process of the ideal gas law at the temperature difference between T_2 and T_1 [55].

$$pV = mRT \quad (\text{Equation 4})$$

$$\frac{T_2}{T_1} = \left(\frac{p_2}{p_1} \right)^{(n-1)/n} = \left(\frac{V_2}{V_1} \right)^{(n-1)} \quad (\text{Equation 5})$$

$$T_2 = T_1 \frac{p_2 V_2}{p_1 V_1} \quad (\text{Equation 6})$$

Thermal efficiency is the ratio of the net work output to the energy input, (Equation 7). Therefore, the thermal efficiency is a good determination of how well the heat is converted into work. This equation can be simplified to actual power output produced by the engine, divided by the rate of energy input (the product of the fuel flow and the fuel lower heating value [LHV]). The thermal efficiency and bsfc definitions are similar; both measure the efficiency of the engine by evaluating fuel input or energy input compared to the actual energy produced. Typical values for standard production SI engines range from peak thermal efficiency and best bsfc of roughly 25% to 35% and 240 g/kWh to 280 g/kWh. Again, these values are for peak engine efficiency, typically we see significantly worse efficiency at idle and low speed low load conditions.

$$\eta = \frac{\dot{W}_{out}}{\dot{Q}_{in}} \quad (\text{Equation 7})$$

$$\eta = \frac{\text{actual power}}{\text{fuel flow} \times \text{LHV}}$$

IMEP is a standard calculation used in combustion analysis and IMEP COV is a good indication of combustion stability. IMEP is essentially a measurement of the engines capacity to do work that is independent of displacement, which permits direct comparison of IMEP values between completely different engines to determine differences or similarities in combustion characteristics. IMEP is determined by first calculating the indicated work per cycle, determined by integrating around the p-V curve (Equation 8). Then, dividing the work per cycle by the cylinder volume obtains IMEP, which is calculated with Equation 9. The IMEP results reported in this thesis are all net IMEP values. The IMEP COV, is calculated as the standard deviation divided by the average (mean) of the IMEP over the statistical window (300 cycles), (Equation 10). A high IMEP COV is undesirable and an important parameter to monitor when studying combustion characteristics for gasoline SI engines.

$$W_i = \oint p dV \quad (\text{Equation 8})$$

$$IMEP = \frac{W}{V_d} \quad (\text{Equation 9})$$

$$IMEP\ COV = 100 \times \frac{StdDev}{Avg} \quad (\text{Equation 10})$$

Combustion duration is the crank angle duration from CA10 to CA90, also represented as Burn1090 (80% of the total mixture burn), and is a part of the rapid-burning angle of the combustion process, (Equation 11). CA10 is the calculated crank angle location where 10% of the combustion process has taken place and CA90 is the crank angle at 90% combustion completion. Combustion duration is the crank angle interval required to burn the bulk of the charge. Benefits of burn rate analysis include its relative simplicity and computation efficiency, so it is commonly used when evaluating combustion. The combustion duration ignores the first and last 10% of the combustion cycle due to their computational difficulties, such as, mixture states, burn mixture composition, motion in the vicinity of the spark plug and energy-release rates being comparable to other energy-transfer processes [54].

$$Combustion\ Duration = CA90 - CA10 \quad (\text{Equation 11})$$

4.2 PEO Coated Piston Inspection following Completion of Testing

The engine was torn down and analyzed after testing, with the status of the PEO-coated piston being the main focus. Inspection of the piston showed reduced heat transfer to the underside of the piston with the PEO coating (Figure 4.12) and no signs of coating deterioration or fatigue after testing completion. The stock piston seen in the left image and the PEO-coated piston is seen in the right image. Hot spots were evident on the stock piston, indicated by burnt oil stains on the underside surface of the piston. The PEO-coated pistons in contrast showed no signs of oil discoloration on the underside, indicating a reduced heat transfer through the piston. Roughly 70 testing hours were conducted on the PEO-coated pistons, a respectable amount of time for

prototype testing of the first coated piston surface iteration. Heat transfer through the pistons is further discussed in section 4.3. Further investigations of piston temperature profiling was not undertaken due to lack of access to either, IR Telemetrics equipment (uses thermocouples imbedded in the piston for real-time temperature measurement), or piston plug temperature equipment (uses temperature sensitive plugs imbedded in the piston for after test measurement) required for analysis, coupled with financial restraints. Upon engine teardown, degradation of the camshaft was also noted; some of the lobes of the camshaft showed increased wear with indentation into the lobes from the lifters. No obvious abnormalities of other engine components were observed.

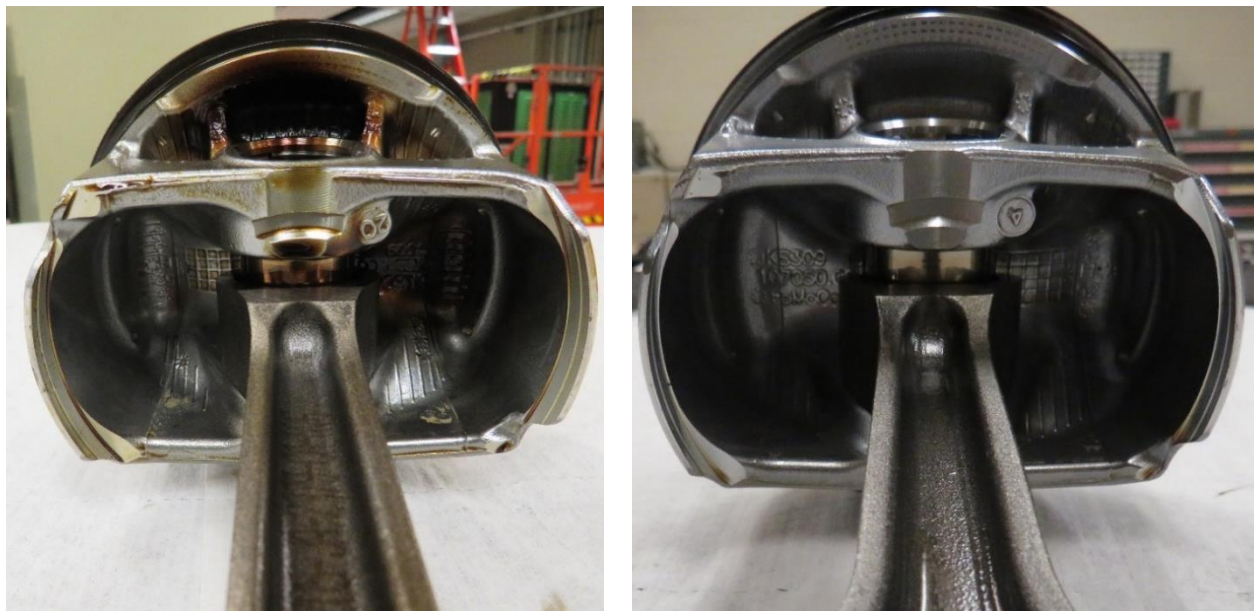


Figure 4.12 - Piston underside after testing completion

4.2 Low Load Analysis and Experimental Results

The low load testing was completed with two different variations of control for the steady state conditions, where the main aim was to compare or match fuel flow and air flow between the stock pistons and PEO-coated pistons. The first variation matched torque values while sweeping the spark and VCT, while in the second variation pedal was kept constant to observe torque

differences. Analysis using both control variations enabled identification of a broader range of potential beneficial aspects.

The engine data was divided into three categories for analysis of low load testing; 1) for standard cell side measurements and engine average (EA) CAS results, all cylinders were used for data presentation, 2) individual bank results were captured with the right bank used for data presentation; 3) for CAS crank angle data, cylinder #1 was used for data presentation because the manifold pressure (MAP) sensor, for pegging, was located in intake runner #1, providing the highest quality results.

The first data set analyzed at low speed, low load conditions was at 1000 rpm 5° VCT retard. This data was summarized in Table 4.5. This data was collected at 2.75 bar BMEP, with the stock IMEP equal to 3.0 bar and the coated piston IMEP equal to 3.25 bar. Stock piston data is observed in black type and PEO-coated piston data is in orange type. As 0° VCT is the most advanced for this engine, testing at 5° introduces very little to no internal EGR from shifting the VCT. For this test run, throttle angles were matched and found the fuel flow and air mass (AM) to be comparable as well. Air mass is the amount of air flowing into the engine. The AFR showed very similar values which are within the error range for the UEGO. Higher torque values were observed with the PEO-coated pistons compared to the stock pistons with the same fuel and air input resulting in a lower calculated bsfc and higher thermal efficiency as shown in Figure 4.13 and Figure 4.14.

Table 4.5 - Steady-state results summary 1000rpm 5° VCT retard low load

Spark Adv [°CA BTDC]	Corrected Torque [Nm]	AFR	Throttle [%]	Exhaust Temperature [°C]	AM [kg/min]	Fuel Flow [kg/h]
31.5	155.9	14.4	8.3	410	1.34	5.6
31	160.4	14.3	8.3	403	1.34	5.6
30.5	156.2	14.4	8.3	415	1.34	5.6
30	160.5	14.3	8.3	408	1.34	5.6
29	160.7	14.3	8.3	411	1.34	5.6
28.5	156.6	14.4	8.3	418	1.34	5.6
28	160.8	14.3	8.3	413	1.34	5.6
26.5	156.7	14.3	8.3	421	1.34	5.6
26	160.1	14.3	8.3	415	1.34	5.6
24.5	155.9	14.4	8.3	425	1.34	5.6
24	159.1	14.3	8.3	419	1.34	5.6

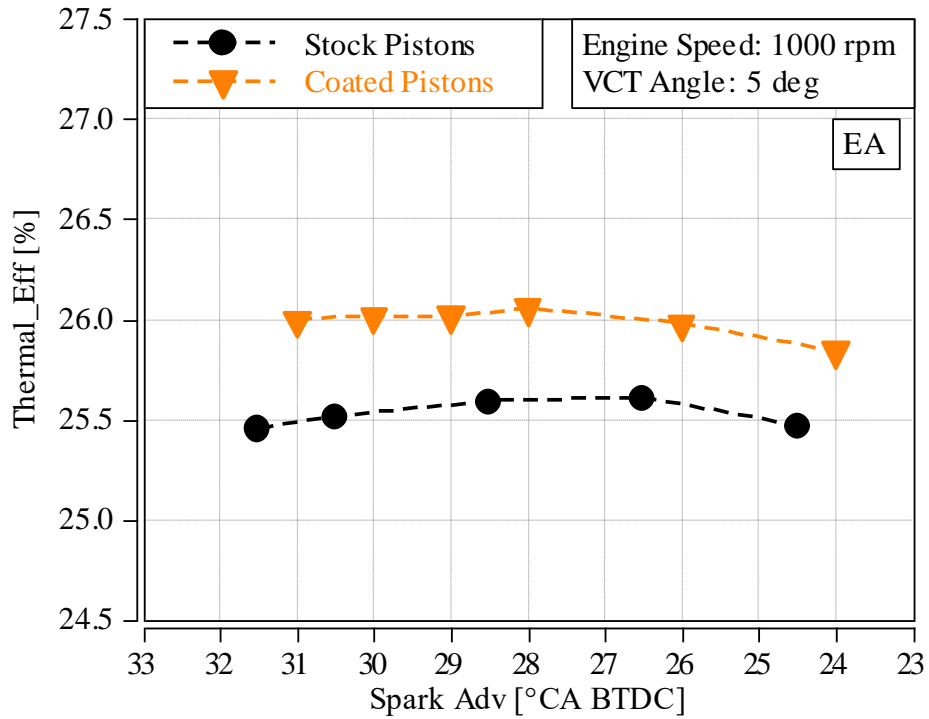


Figure 4.13 - Thermal efficiency versus spark advance at 1000 rpm 5° VCT retard

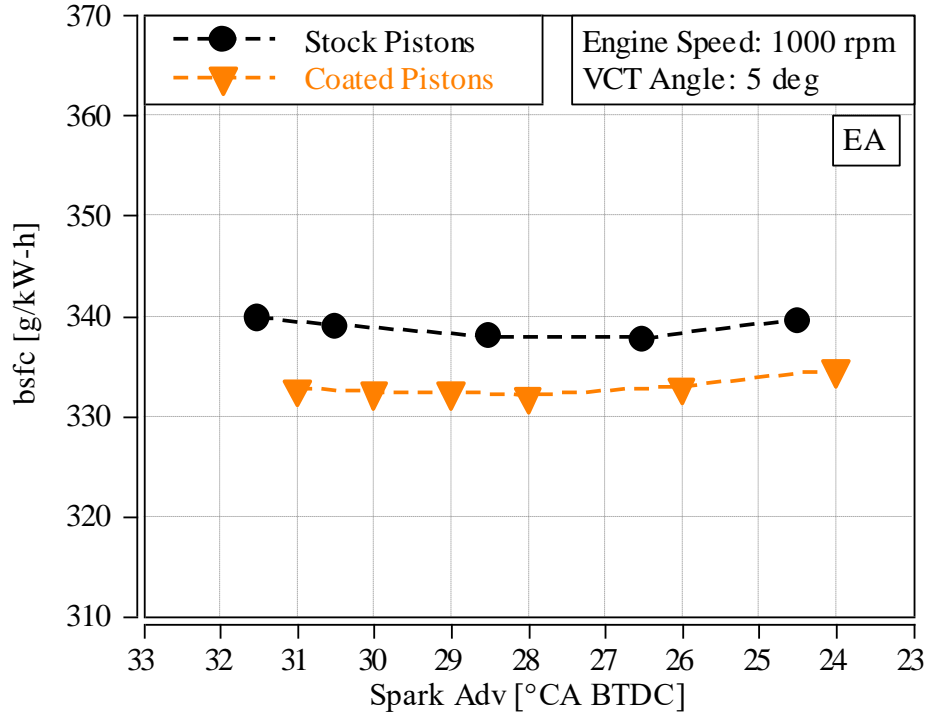


Figure 4.14 - bsfc vs spark advance at 1000rpm 5° VCT retard

The improved efficiency and higher torque output observed with the PEO-coated pistons compared to the stock pistons at low loads, suggests more energy was used on the piston during expansion, supporting the theorized increased heat retention capabilities of the PEO coating.

Table 4.5 shows the exhaust temperatures are slightly lower for the coated pistons compared to the stock pistons. Similar exhaust temperature results were observed in other low load, low engine speed conditions with the PEO coated pistons in this study.

HRR follows the pressure traces and the bulk gas temperatures shadow the differences observed in the HRR. In Figure 4.15 and Figure 4.16 the combustion cycle was observed and the differences in the rapid flame burning stage between the PEO-coated and stock uncoated pistons. The slightly higher HRR supported the higher efficiency and lower bsfc, which means more work was used during the expansion stroke. The flame-development angle region and end of flame propagation angle showed little change between the stock piston and the coated piston, but are not the area of focus for this study. The PEO-coated pistons show reduced variability of HRR based on spark timing compared to the stock pistons, resulting in a more consistent, stable combustion over a

wider range. Slightly higher bulk gas temperatures were observed following the higher HRR and cylinder pressure traces. These results were expected as the PEO coating acts as a very good thermal barrier. With the same energy input and the observed higher heat release rates and higher bulk gas temperature, there was less heat loss through the piston surface during the combustion cycle. All cylinders showed similar results, but as previously noted cylinder 1 was the main comparison cylinder for quality assurance purposes.

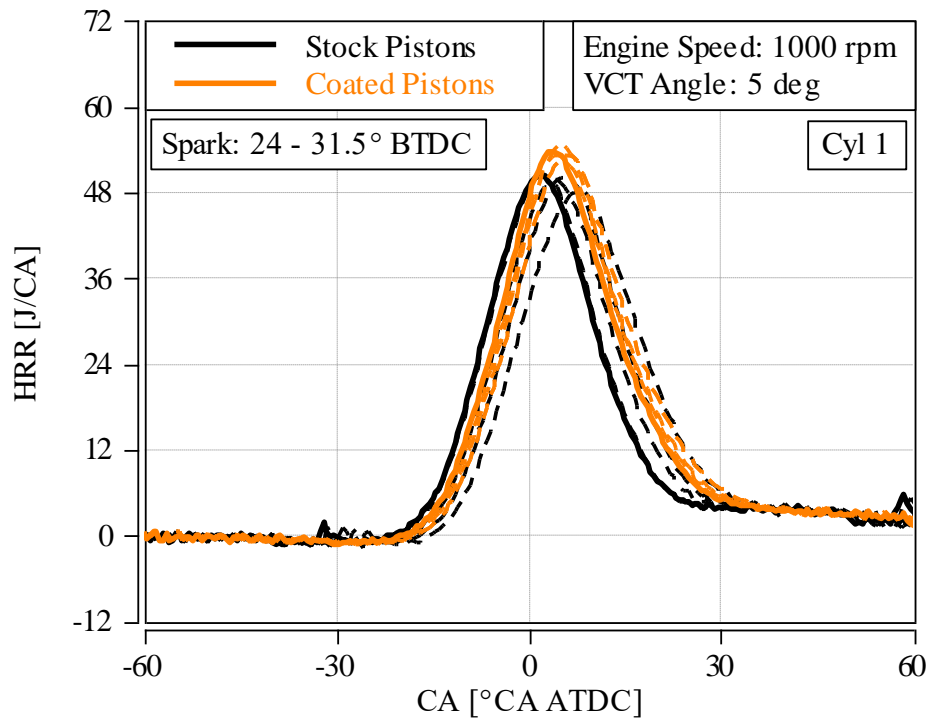


Figure 4.15 - Heat Release Rate at 1000rpm 5° VCT retard spark sweep

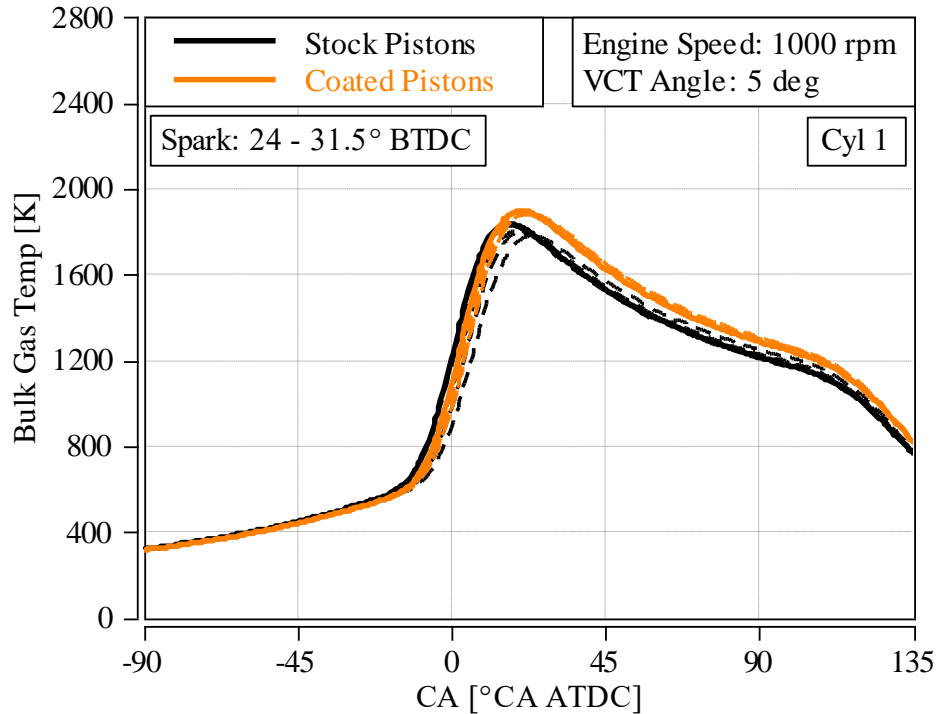


Figure 4.16 - Bulk Gas temperature at 1000rpm 5° VCT retard spark sweep

The purpose of calculating the bulk gas temperatures is to determine if the temperature change results from less heat transfer through the PEO-coated pistons. The higher bulk gas temperatures observed is beneficial only if the expansion work can be increased, and not lost out the exhaust after the combustion cycle. The results of increased thermal efficiency, reduced bsfc, increased torque while maintaining constant air and fuel input, collectively supports the expectation of reduced heat transfer through the PEO-coated piston and increased extraction of inputted energy. The data showed a closer spread of bulk gas temperatures same as the HRR curves.

Plotting the Log p vs Log V helps with data quality checks and shows where there are gains or losses because it visually assists in dividing the combustion cycle between the intake, compression, expansion and exhaust stroke. In Figure 4.17, no differences were observed during the intake, compression and exhaust strokes but slightly elevated Log p pressures during the expansion stroke were seen. This correlates with the higher bulk gas temperatures as well indicating there is more usable energy during the combustion cycle.

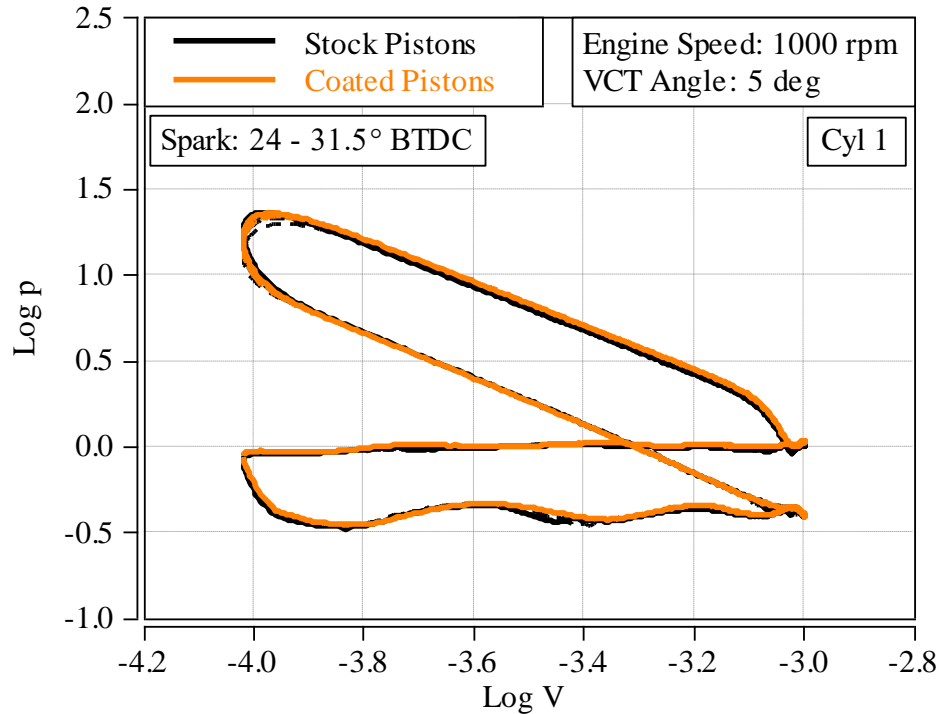


Figure 4.17 - Log p vs Log V at 1000rpm at 5° VCT retard spark sweep

The combustion duration was reduced with the PEO-coated pistons at the more advanced spark values compared to the stock pistons (Figure 4.18). A shorter combustion duration is favorable as a fast combustion correlates to increased cycle work done during the expansion stroke and reduced heat loss to the combustion chamber. Since heat transfer is a time-based event for the combustion cycle, the faster the heat release the less heat or energy lost and unavailable for use. Therefore, a shorter combustion duration as observed with the PEO-coated pistons, is more desirable.

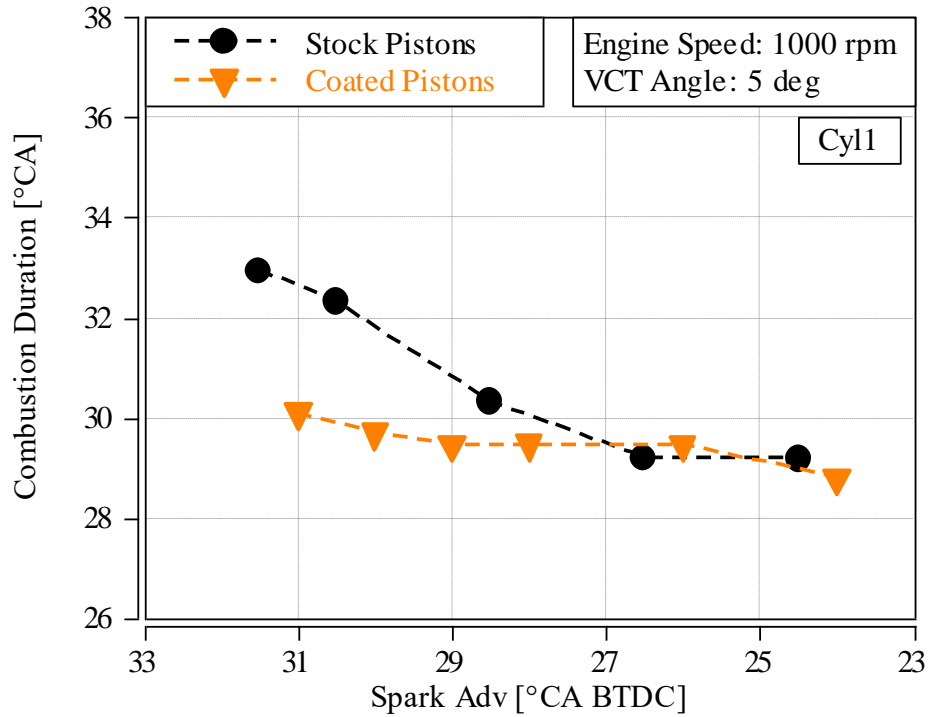


Figure 4.18 - Combustion duration coated piston vs uncoated at 1000rpm 5deg VCT retard spark sweep

IMEP COV, as previously noted, is an important calculation to observe when studying combustion of gasoline SI engines. Typically, gasoline SI engines have relatively high IMEP COVs, especially at low load, low speed conditions. Thus, it is important to determine if there is improvement or, at minimum, no degradation of the IMEP COV with the PEO-coated pistons. Figure 4.19 shows the IMEP COV comparing the stock pistons to the PEO-coated pistons; similar results were observed between the pistons. The ideal outcome would be improved IMEP COVs with the potentially higher in-cylinder temperatures. Combustion is least stable with the highest IMEP COVs during cold starts and cold operating conditions, theorizing increased combustion chamber temperatures would improve combustion stability leading to decrease IMEP COV results.

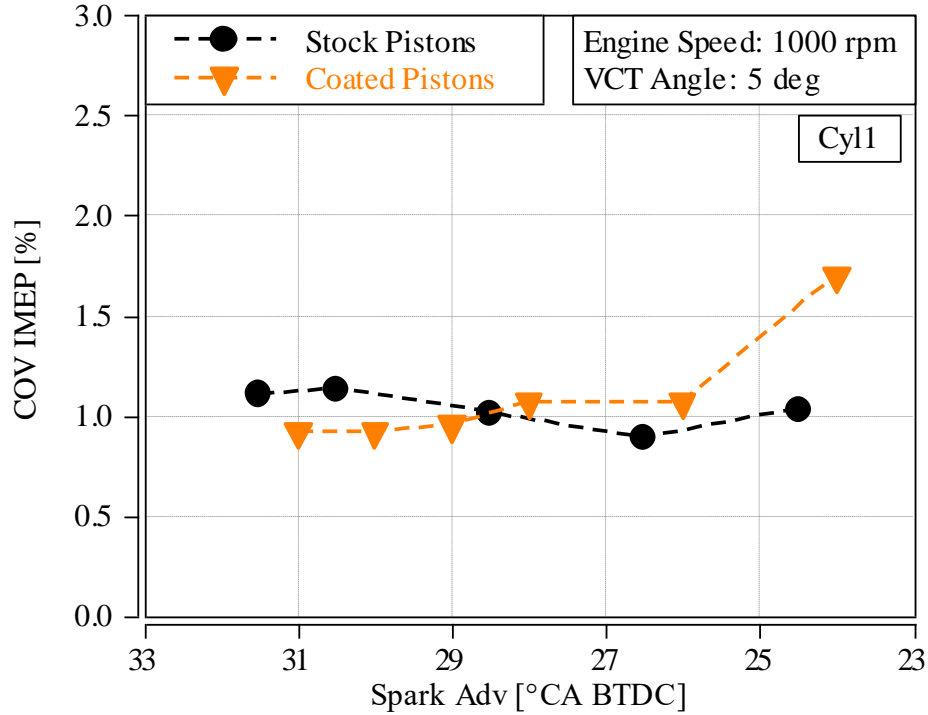


Figure 4.19 - IMEP COV coated piston vs stock piston spark sweep at 1000rpm 5 VCT° retard

The beneficial results with the PEO coating obtained at 1000rpm and 5° VCT low load conditions unfortunately, are not mirrored at other speeds, loads, VCT angles and spark advance settings. As mentioned earlier the 5° VCT retard is close to the most advanced setting for this engine. As the VCT was retarded a small amount of internal EGR was introduced, since it is a single camshaft resulting in a dual equal intake and exhaust retard. The overlap doesn't change but the result is the intake valve opens later and closes later allowing small amounts of combustion gases to back flow into the intake. There is also, less exhaust gas blowdown with a later exhaust valve opening and closing trapping more exhaust gasses in the cylinder. When retarding the VCT and introducing small amount of internal EGR the engine IMEP COV can deteriorate as combustion becomes more unstable.

Increasing speed to 1500rpm and retarding the VCT angle to the highest allowed angle, 50° VCT retard, did not reproduce the results obtained at 1000rpm 5° VCT retard. The summarized data can be seen in Table A.6 with the BMEP equal to 4.5bar. The stock piston IMEP was 4.75bar and coated-piston IMEP 5.0 bar. Stock piston data is in black type and PEO coated piston data is in

orange type. There was no difference found in the thermal efficiency, (Figure 4.20), or bsfc, (Figure A.33), between the PEO-coated and stock pistons. It is possible there are complications with the distribution at these levels of VCT retard, resulting in, uneven results piston-to-piston, causing the potential improvements to be canceled out (Figure A.35 to Figure A.41).

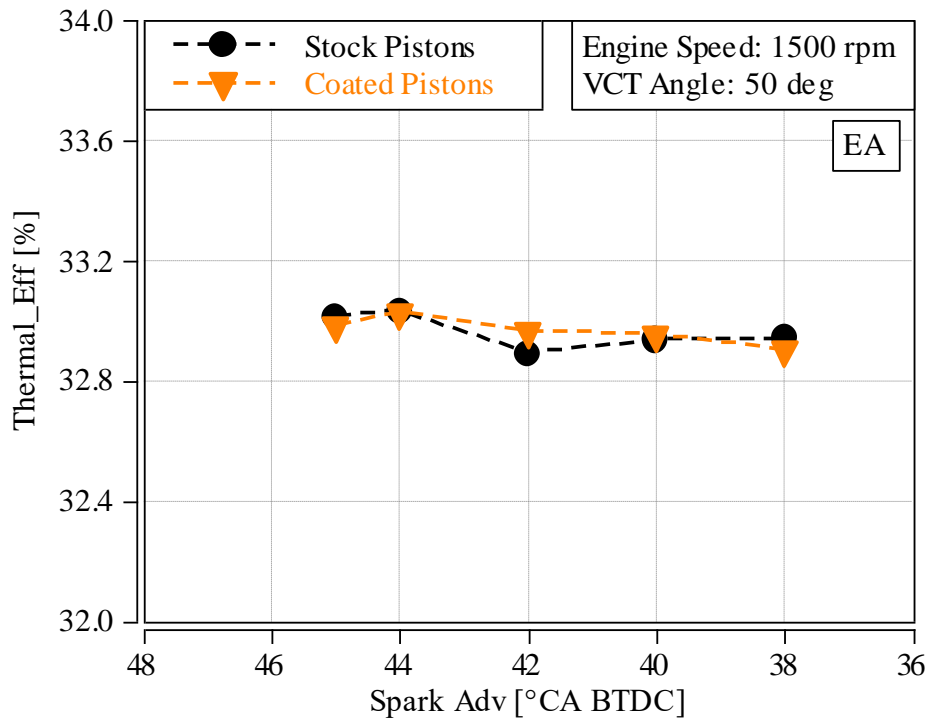


Figure 4.20 - Thermal efficiency versus spark advance at 1500 rpm 50° VCT retard

A slight increase in bulk gas temperatures was obtained with the PEO-coated pistons, shown in Figure 4.21, but this increased energy was unable to be used on the piston during the expansion stroke. The HRR showed similar results as the bulk gas temperatures, Figure A.34. This assumption was made because the HRR and bulk gas temperatures show elevated curves for the PEO-coated pistons compared to the stock pistons, indicating there is more heat and energy in the combustion chamber during the expansion stroke. However, the bsfc and thermal efficiency do not show improvements were observed.

Camshaft wear, which was observed with engine tear down at study completion, may have also partially negated the positive impacts derived from the PEO-coated pistons. The camshaft wear was not a result of the PEO coating of the pistons but rather a flaw in the camshaft design, or possibly a random error in installation of the camshaft and camshaft bearings, resulting in accelerated deterioration of a couple of camshaft lobes. The wear on the camshaft lobes would increase friction and pumping, negatively influencing testing conducted at the increased speeds and loads. The increased friction would be more influential at higher speeds, in keeping with the slight improvements observed at low speed, but not higher speed testing conditions.

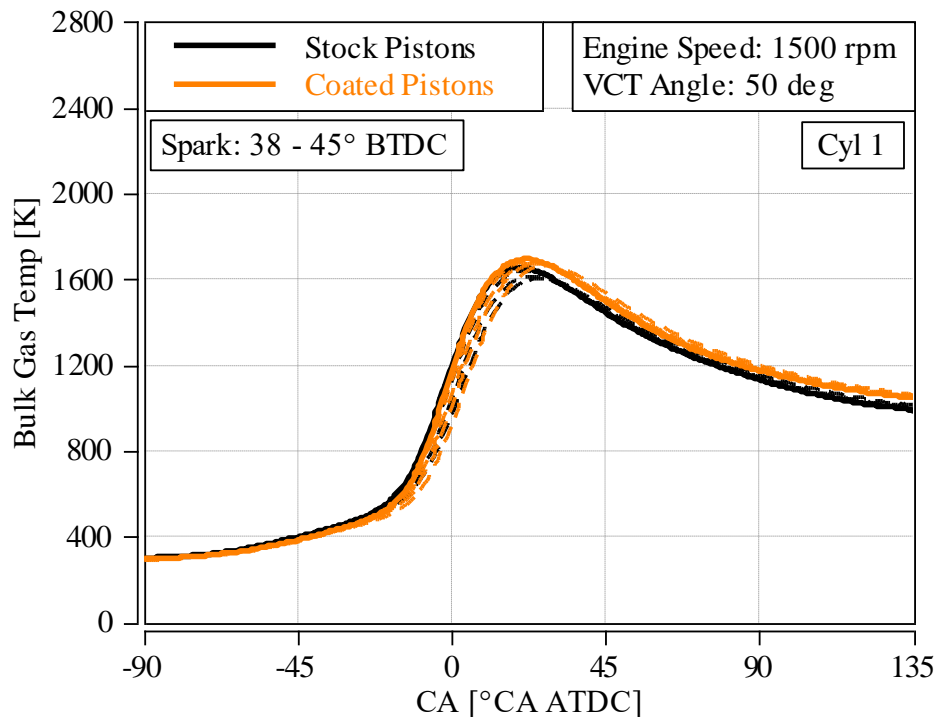


Figure 4.21 - Bulk Gas temperature at 1500rpm 50° VCT retard spark sweep

In contrast to the apparent absence of impact of PEO-coated pistons on thermal efficiency, bfsc and the minimal impact on bulk temperatures, the coating did favorably influence the IMEP COV. Figure 4.22 shows a decreased IMEP COV at more advanced spark timing for the PEO-coated versus stock pistons. The maximum VCT retard, for any setup, will typically cause higher IMEP COV conditions. Improved IMEP COV will help with emissions reduction because reduced

combustion variability will decrease the possibility of intermittent lean or rich combustion events, increasing one or more of the exhaust emission gases. IMEP COV plays a key role in NVH as well with a lower IMEP COV giving better NVH results.

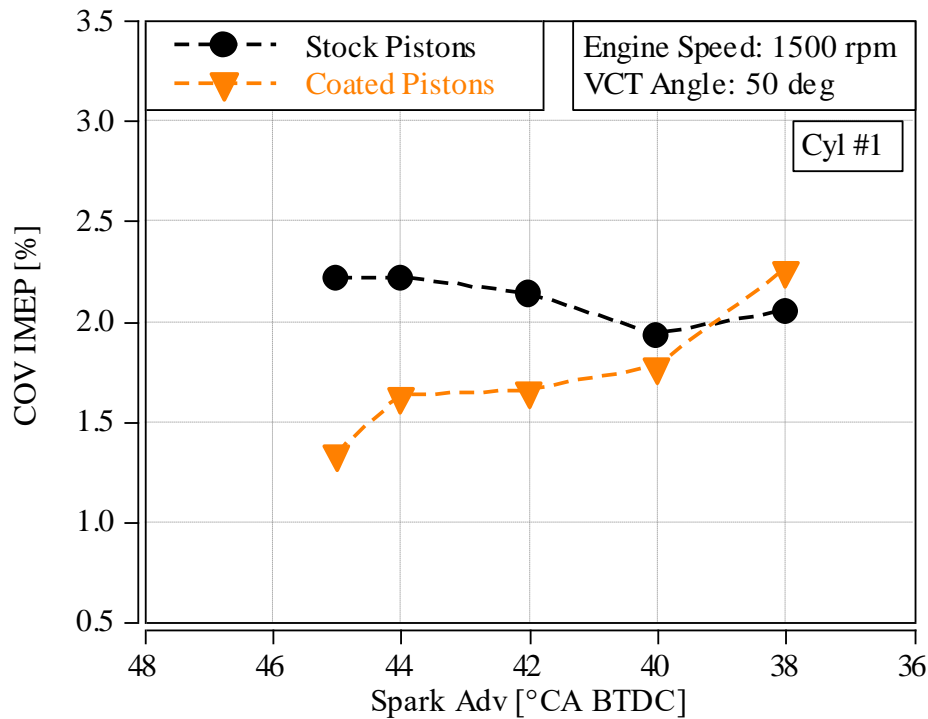


Figure 4.22 - IMEP COV coated piston vs stock piston spark sweep at 1500rpm 50° VCT retard

4.3 High Load Analysis and Experimental Results

High load testing was completed at various speeds close to peak power and peak torque. Spark sweeps were performed at various VCT angles as for the low load testing, to analyze the differences of combustion with increased heat retaining potential of the PEO-coated pistons. The aim of the full load, high speed analysis was to determine if power and torque would be affected with less heat transfer across the pistons, potentially resulting in an increased amount of usable energy, or whether the output would remain unaffected. Testing revealed a negative impact of the PEO coating; a high knocking tendency was observed at all speeds and VCT angles for the coated pistons compared to the stock pistons.

Knock is the auto-ignition of end gases. End gases are the unburned portion of the mixture in the combustion chamber ahead of the advancing flame front. Auto-ignition causes end gases to burn rapidly, releasing energy at a rate 5 to 25 times the rate achieved during normal combustion. This rapid release of energy causes high-pressure oscillations inside the combustion chamber, which can produce an audible noise associated with heavy knock.

During testing the cause of higher knocking tendencies were speculated and appropriate assessments were undertaken. Increased thermal barrier properties of the PEO coating should be reducing the cooling effect through the piston. This is either causing excessive heating of the crown of the piston, or the bulk gas temperatures of the charge are increasing to higher temperatures than the octane of the fuel can handle to prevent pre-ignition of the end gases. The piston typically dissipates a large amount of heat through it, hence the need for piston squirters. This engine runs a single piston squirter but other current production engines running at very high stresses can run up to 3 piston squirters per piston. The squirters serve two purposes: 1) to cool the piston to prevent fatigue due to the high temperatures exerted on them and, 2) to cool the piston so as to prevent creating a large hot surface in the combustion chamber, thereby preventing the risk of knocking. A result of the massive heat transferred through the stock piston can be observed in Figure 4.23. Dark brown staining, which is burnt oil, is observed on the underside of the stock piston due excess heat transferred through the piston. The dark brown areas to the left of the wrist pin and at the top of the image are the result of burnt oil staining on the underside of the stock piston. However, in contrast, as noted previously (section 4.1, Figure 4.12), at engine tear down, the PEO-coated piston did not show any signs of excessive heat transfer through the piston.



Figure 4.23 - Stock piston underside

Due to the knock tendencies I could not match the same spark advance values or CA50 values for the PEO coated pistons, that could be obtained with the stock pistons. Higher knock peak-to-peak values were observed at all speeds, VCT angles with the PEO-coated pistons and the amplitudes of knock increased significantly when trying to match the same spark values. Figure 4.24 and Figure 4.25 show the higher knock peak-to-peak values for the PEO-coated pistons compared to the stock pistons, correlating with a higher knocking tendency. All 8 cylinders are plotted for both the reference data and PEO-coated piston data to demonstrate the spread across all cylinders and verify knock is consistent. Increased fuel enrichment was required to reduce exhaust temperature limits since spark retard was required to reduce knocking. Knocking was consistent amongst all operating variations, VCT angles 0° – 15° exhaust retard, and found to be more aggressive at higher speed and more retarded VCT angles.

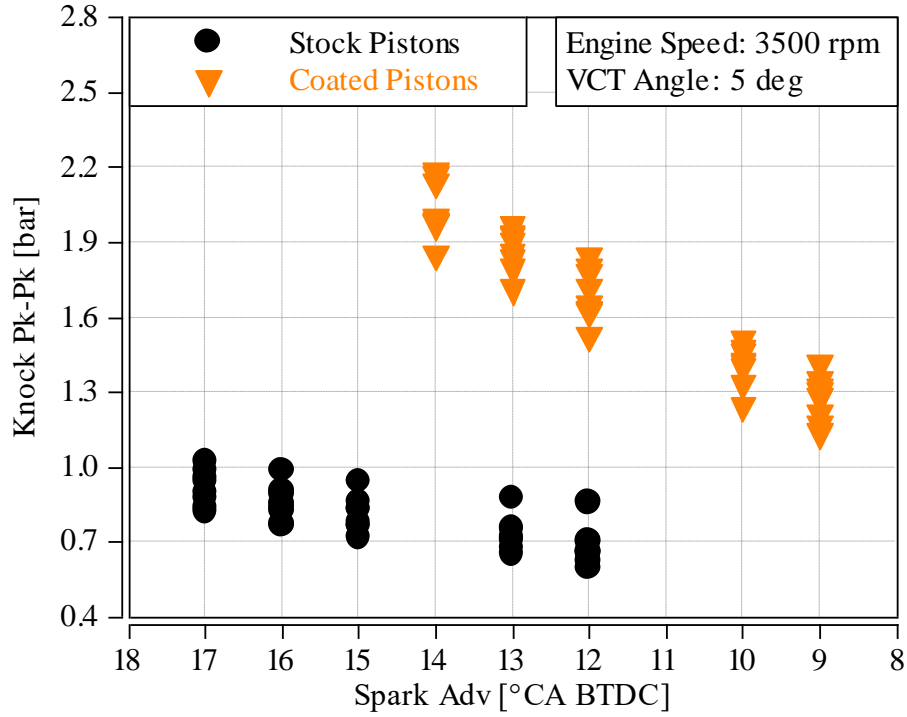


Figure 4.24 - Knock peak-to-peak 3500rpm full/high load 5° VCT retard

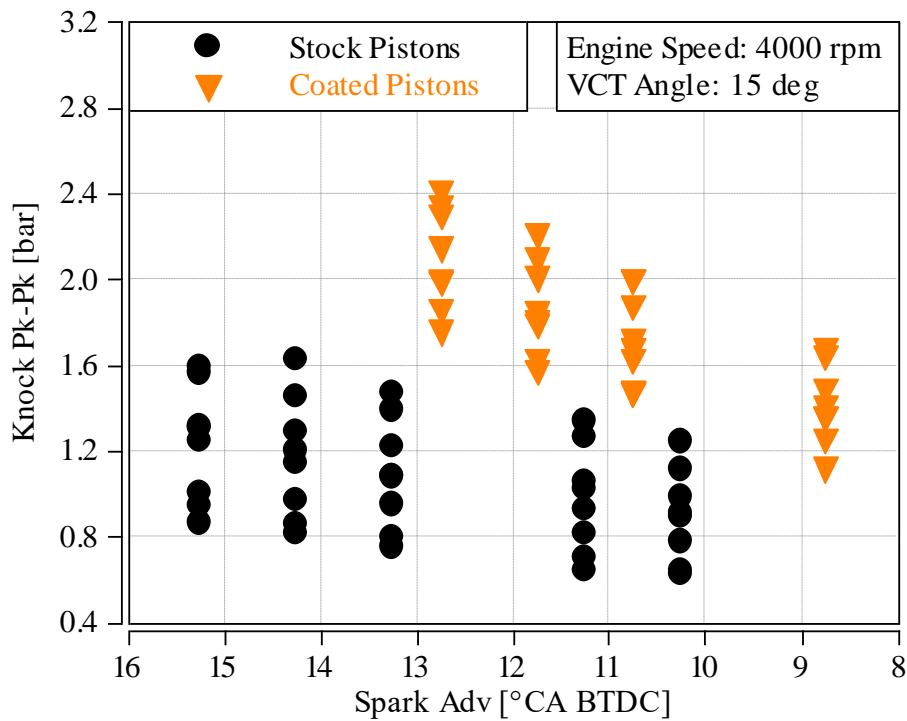


Figure 4.25 - Knock peak-to-peak 4000rpm full/high load 15° VCT retard

The knock value of the PEO-coated pistons was shown to be higher relative to the stock pistons. However, any knock peak-to-peak value above 1.5 is indicative of mild pressure oscillations indicating a possible knock presence. Values of knock peak-to-peak above 2 correlates with moderate to high oscillations indicating an upper threshold that, for our testing purposes, I did not want to exceed. Audible knock is considered very heavy knock and would be observed at higher values and cause visible damage to the combustion chamber or pistons.

Figure 4.26 shows the knock peak-to-peak at 3500rpm 10° VCT retard and shows similar results to 3500rpm 5° VCT. With the retarded spark timing the resulting CA50 was retarded and the engine was not able to run at its optimum efficiency or maximum brake torque MBT spark timing. This in turn affects the bsfc and thermal efficiency in a negative manner, resulting in lower thermal efficiency and higher bsfc. The fueling had to be enriched for exhaust temperature limit purposes due to the retarded spark timing, negatively impacting combustion efficiency outcomes. Had the fueling not required enrichment, the thermal efficiencies and bsfc would theoretically be comparable to the stock pistons setup.

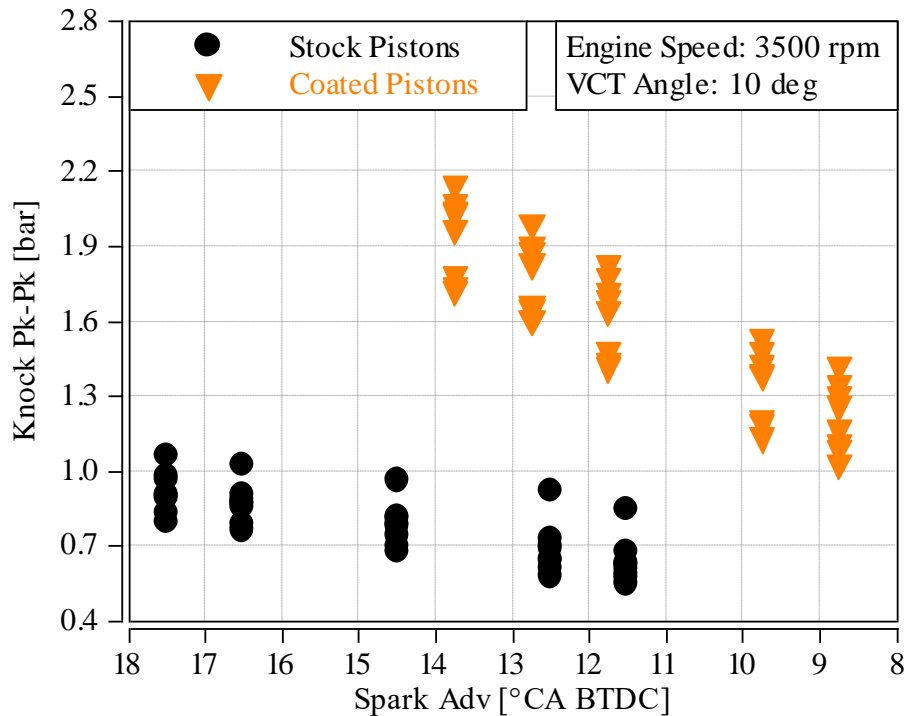


Figure 4.26 - Knock peak-to-peak 3500rpm full/high load 10° VCT retard

Review of the HRR traces in Figure 4.27 make it apparent that, due to the knock limitations, it is difficult to use the extra heat trapped by the PEO-coated pistons during the expansion stroke, to extract more work from the combustion cycle. Looking closely at the overlap of spark timing for the HRR traces, the PEO-coated pistons produce slightly higher HRR curves, indicating there is potential for higher work during the expansion stroke. However, the farther away from the ideal CA50 of 7° ATDC, the worse the efficiency, which is standard for every IC engine. The CA50 target of close to 7° ATDC should be achievable for this engine, since stock operation is in the region of CA50 10° ATDC. The cylinder pressure traces in Figure 4.28 show that for the same spark, the PEO-coated pistons achieve slightly increased cylinder pressures. However, overall the stock piston was able to achieve higher cylinder pressure and HRRs because of the more advanced spark timing. This suggested that the reason for the higher knock tendencies is not necessarily the bulk gas temperatures or pressures exceeding the pre-ignition temperatures of the fuel, but the piston crown becoming a surface area with such increased heat, that it was causing auto-ignition of the end gas mixture before the flame front propagated to the piston crown. In this case, when the bulk charge reaches the piston surface the charge mixture or the micro-oil particles are igniting the end-gases before the flame front can reach that location, causing knocking. The PEO-coated pistons thermal barrier properties do not allow for the cooling of the piston jets to pass through to the surface of the piston. In this case, the coated-piston surface would be hotter than the stock pistons.

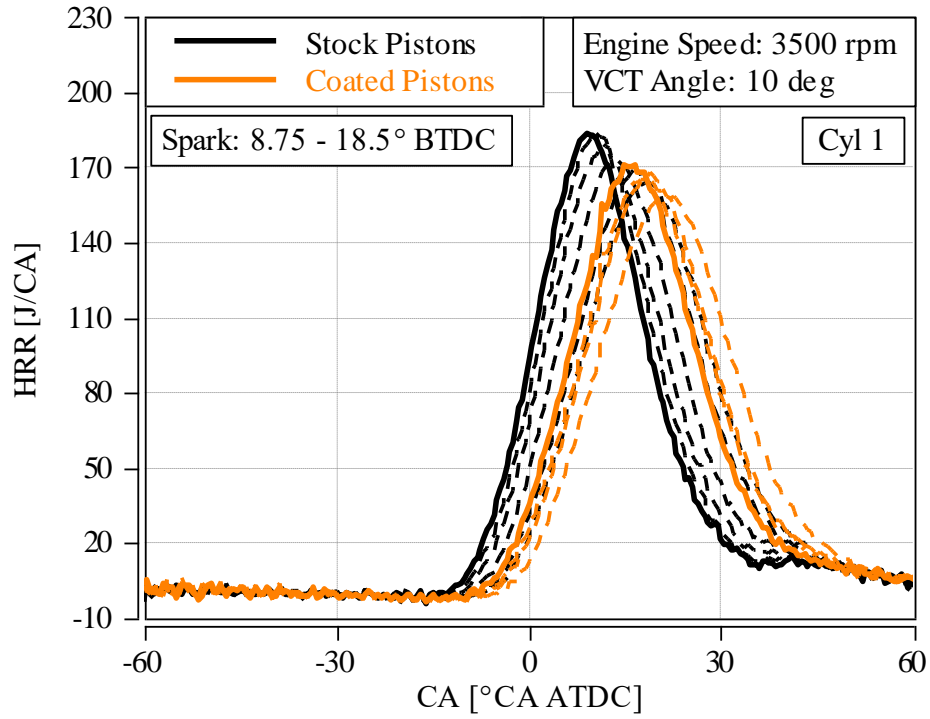


Figure 4.27 - Heat Release Rate at 3500rpm 10° VCT retard full load spark sweep

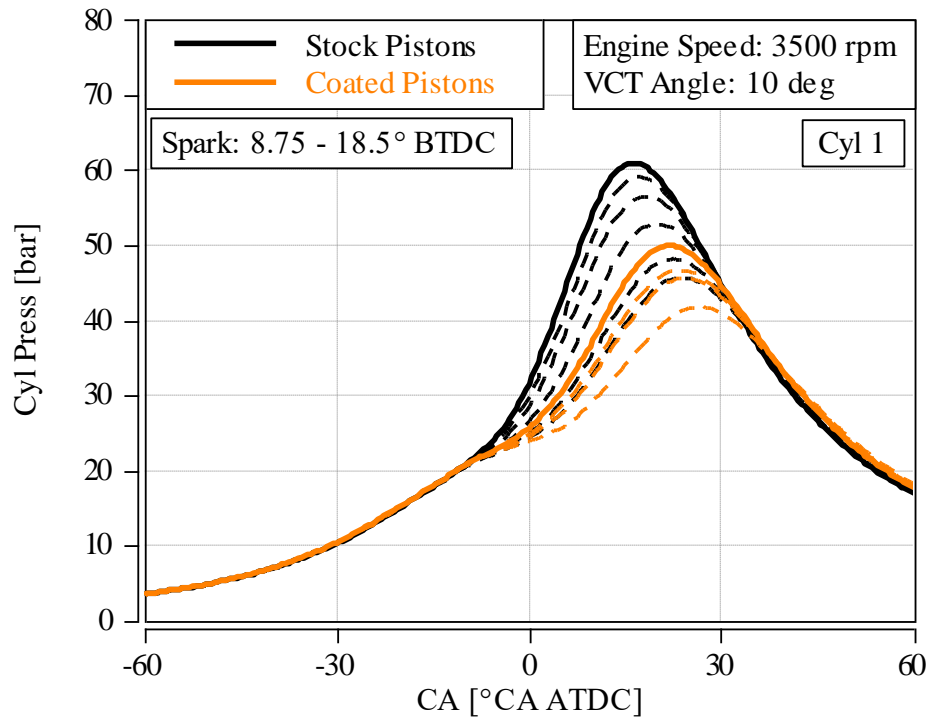


Figure 4.28 - Cylinder pressure traces at 3500rpm 10° VCT retard spark sweep

Comparing the PEO-coated and uncoated pistons, factoring out the fuel enrichment required, the estimated efficiencies are theoretically comparable. The projection of the thermal efficiency would require further experimentation as the relationship is not linear and there are multiple heat transfer factors involved when estimating this relationship. However, plotting and extrapolating to visualize the estimated difference in efficiency, Figure 4.29, the trendline shows a line of best fit for the thermal efficiency with the PEO-coated pistons as the spark timing is advanced. Therefore, if the knocking tendencies can be mitigated, and required fuel enrichment reduced, allowing for comparable spark timing at higher normal operating conditions, further analysis may show beneficial outcomes.

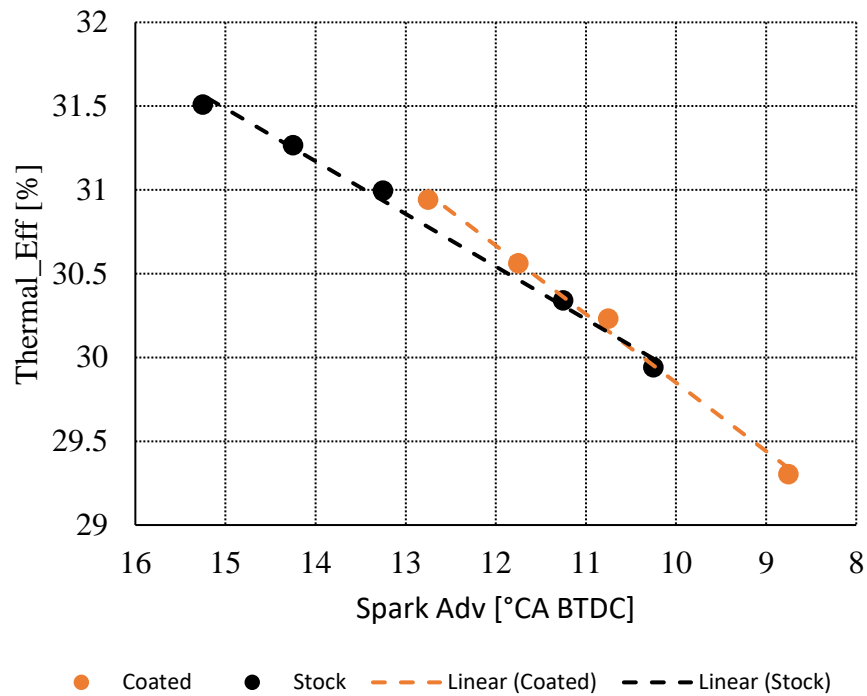


Figure 4.29 - Estimated thermal efficiency extrapolated at 3500rpm 10° VCT full load

CHAPTER 5 CONCLUSIONS AND RECOMMENDATIONS

5.1 Conclusions

The presented work discussed the research undertaken assessing the effect of PEO-coated pistons on combustion in SI internal combustion PFI with VCT capability engines. The properties of PEO coatings, including high wear and corrosion resistance, high hardness, excellent adhesion and superior thermal barrier capabilities confer potential advantages for their use in the SI ICE. The objective of the research was to investigate the impact PEO coatings of stock Al alloy pistons have on combustion in a SI ICE for the purpose of improved efficiency to meet industry targets demanding reduced carbon emissions and fuel consumption.

Testing was conducted on a 7.3L Ford engine fitted with stock Al alloy pistons followed by in-house PEO-coated pistons. An AC Medien Dynamometer and an A&D Pheonix AM/RT combustion analysis system using real-time in-cylinder pressure data coupled with the dynamometer cell data were used to analyze low load and high load conditions.

The conclusions of the research are summarized as follows:

1. The PEO-coated pistons provided minor benefits compared to the stock pistons at low load and low speed conditions. Improved bsfc and thermal efficiency with increased HRR and bulk gas temperatures were observed with the PEO-coated pistons. The PEO-coated pistons also favorably influenced the IMEP COV.
2. These benefits did not project further onto retarded VCT angles, higher speeds and loads. PEO-coated pistons did not change thermal efficiency, bfsc and had minimal positive impact on bulk gas temperatures.
3. The PEO-coating negatively impacted engine performance when tested at peak torque and power speeds at full load, due to the complicated effect from thermal conductivity of the PEO-coating.
4. Careful consideration of the data suggested that the reduced heat transfer through the piston cause a heated piston crown and the end gas combustion charge mixture to ignite before the flame front reached it.

5. Increased fuel enrichment was required to prevent damage from increased temperatures induced by spark retard to enable continued testing at peak torque and power speeds at full load.
6. Projections suggested the potential for improvement if engine limit conditions could be extended and knock tendencies reduced.

5.2 Recommendations for Future Work

Although the benefit derived from the use of PEO coating on pistons was observed only in limited engine test conditions, the data collected and analyzed in this thesis provide direction for future study to continue to explore the potential advantages of PEO-coated pistons.

The future work recommendations are summarized as follows:

1. Evaluate motoring curves. This would enable analysis solely of the heat transfer properties of the coating with the reduced variability of combustion. This would decrease the complexity of heat transfer calculations, reducing the number of assumptions required.
2. Evaluate cold start conditions. Cold start functions were not addressed in this study, but potential stability benefits could be observed if more heat can be trapped and used in the combustion chamber, with the potential for reduced emissions. PEO-coated pistons provide better thermal properties with the ability to trap more heat in the combustion chamber.
3. Use higher-octane fuels or biofuels. Negative effects of the PEO-coated pistons were observed at higher load and engine speeds due to knock limitations of the SI engine and engine temperature limitations. Therefore, exploring the PEO-coated piston capabilities using higher-octane fuels with lower pre-ignition properties to prevent knocking, may reveal improved performance.
4. Seal the porous surface of the PEO-coated piston with a high silicate sealer. Studies have shown PEO coatings with silicate surface sealing on CI ICEs achieve beneficial results because the silicate sealing penetrates the pores on the coating surface, thereby reducing the roughness [3]. This would decrease the amount of unburned end-gases getting trapped in the PEO-coating pores, potentially reducing the temperature of the theorized super-heated piston crown or hot spots formed on the piston surface.

5. Selective coating of specific areas on the piston crown. Studying and analyzing the tumble effect of the air-fuel mixture in the cylinder along with the flame-front propagation during mixing and combustion could reveal areas of the piston crown that are more prone to knocking. The study of the flame-front propagation would reveal the areas of the piston crown that are reached first and last. Therefore, selective coating could provide benefits of good thermal barrier properties, mitigating the knock tendencies, which hinder the full load, high speed performance [3].
6. Thinner coating thickness. Current coating thickness for this testing was relatively thick, at roughly 100 μ m, producing excellent thermal barrier properties. A thinner coating of roughly 30-50 μ m will permit some heat penetration to and through the substrate material. This would potentially prevent the development of the piston crown becoming a hot spot, thereby mitigating knock tendencies, while still allowing less heat transfer from combustion to the combustion chamber.
7. Coat the exhaust valves and other engine components. PEO-coating will avoid the temperature limitations of the engine components and could show improvements where, in the study, negative factors were observed.
8. Reduce the substrate material thickness. The extremely low conductive heat properties of PEO coatings could allow for reduced crown thickness, since heat transfer to the substrate is massively reduced. Assuming structural integrity is sufficient, a reduction of crown thickness combined with the PEO coating could potentially reduce rotational mass and inertia, thereby increasing responsiveness performance. Durability testing would be required to ensure no piston surface degradation.
9. Perform internal piston temperature testing for full piston temperatures profiling. Since PEO coatings reduce the temperature transferred to the piston substrate, a full real-time temperature profile study of the piston would reveal the benefits and areas for improvement. For example, PEO coating could possibly remove the requirement for piston squirters, decreasing power robbed by the oil pump and increasing fuel efficiency. The piston squirters are a large power consumer in CI diesel engines. Furthermore, durability is critical to the operation of big diesel engines and preventing excessive piston heating is essential to durability.

This work could then be further extrapolated upon to find the best combination of coated components in ICEs, determining if CI or SI has the potential to show the most improvement and what fuel type would assist in producing the best results. The combination chosen would need to yield the largest gains in efficiency, reduction of emissions, fuel consumption and reduced friction.

REFERENCES

- [1] "EPA United States Environmental Protection Agency," December 2021. [Online]. Available: <https://nepis.epa.gov/Exe/ZyPDF.cgi?Dockey=P1013NR8.pdf>. [Accessed May 2022].
- [2] "EPA United States Environmental Protection Agency," December 2021. [Online]. Available: <https://nepis.epa.gov/Exe/ZyPDF.cgi?Dockey=P1013NRF.pdf>. [Accessed May 2022].
- [3] A. Hegab, K. Dahuwa, R. Islam, A. Cairns, A. Kurana, S. Shrestha and R. Francis, "Plasma electrolytic oxidation thermal barrier coating for reduced heat losses in IC engines," *Applied Thermal Engineering*, vol. 196, no. 117316, pp. 1359-4311, 2021.
- [4] D. Gatti and M. Jansons, "One-Dimensional Modelling and Analysis of Thermal Barrier Coatings for Reduction of Cooling Loads in Military Vehicles," SAE International Technical Paper, 2018.
- [5] R. Kamo, D. N. Assanis and W. Bryzik, "Thin Thermal Barrier Coatings for Engines," SAE International Technical Paper, 1989.
- [6] G. Woschni, W. Spindler and K. Kolesa, "Heat Insulation of Combustion Chamber Walls — A Measure to Decrease the Fuel Consumption of I.C. Engines?," SAE International in United States, 1987.
- [7] W. GEBAROWSKI and S. PIETRZYK, "Growth Characteristics of the Oxide Layer on Aluminum in the Process of Plasma Electrolytic Oxidation," *Archives of Metallurgy and Materials*, vol. 59, no. 1, pp. 407-411, 2014.
- [8] B. L. Jiang and Y. M. Wang, "Plasma electrolytic oxidation treatment of aluminium and titanium alloys," in *Surface Engineering of Light Alloys*, Woodhead Publishing, 2010, pp. 110-154.
- [9] M. Aliofkhazraei and A. S. Rouhaghdam, *Fabrication of nanostructures by plasma electrolysis*, Weinheim, 2011.
- [10] R. O. Hussein, X. Nie and D. O. Northwood, "The Application of Plasma Electrolytic Oxidation (PEO) to the Production of Corrosion Resistant Coatings on Magnesium Alloys," *Corrosion and Materials*, vol. 38, no. 1, pp. 53-63, 2013.
- [11] L. O. Snizhko, A. L. Yerokhin, A. Pilkington, N. L. Gurevina, D. O. Misnyankin, A. Leyland and A. Matthews, "Anodic processes in plasma electrolytic oxidation of aluminium in alkaline solutions," *Electrochimica Acta*, vol. 49, pp. 2085-2095, 2004.

- [12] A. L. Yerokhin, X. Nie, A. Leyland, A. Matthews and S. J. Dowey, "Plasma electrolysis for surface engineering," *Surface and Coatings Technology*, vol. 122, p. 73–93, 1999.
- [13] F. Simchen, M. Sieber, A. Kopp and T. Lampke, "Introduction to Plasma Electrolytic Oxidation—An Overview of the Process and Applications," *Coatings MDPI*, vol. 10, no. 7, 2020.
- [14] M. Marr, J. S. Wallace, S. Memme, S. Chandra, L. Pershin and J. Mostaghimi, "An Investigation of Metal and Ceramic Thermal Barrier Coatings in a Spark-Ignition Engine," *SAE International Journal of Engines*, vol. 3, no. 2, pp. 115-125, 2010.
- [15] R. O. Hussein, D. O. Northwood and X. Nie, "Coating Growth Behavior During the Plasma Electrolytic Oxidation Process," *Journal of Vacuum Science and Technology A*, vol. 28, no. 4, pp. 766-773, 2010.
- [16] R. O. Hussein, X. Nie and D. O. Northwood, "Effect of cathodic current density on the corrosion protection of the oxide coatings formed on AZ91D magnesium alloy by plasma electrolytic oxidation," *Corrosion and Prevention*, vol. 112, 2013.
- [17] R. O. Hussein, D. O. Northwood, J. F. Su and X. Nie, "A study of the interactive effects of hybrid current modes on the tribological properties of a PEO (plasma electrolytic oxidation) coated AM60B Mg-alloy," *Surface & Coatings Technology*, vol. 215, pp. 421-430, 2013.
- [18] F. Simchen, M. Seiber and T. Lampke, "Electrolyte influence on ignition of plasma electrolytic oxidation processes on light metals," *Surface Coating & Technology*, no. 315, pp. 205-213, 2017.
- [19] B. Kasalica, J. Radić-Perić, M. Perić, M. Petković-Benazzouz, I. Belča and M. Sarvan, "The mechanism of evolution of microdischarges at the beginning of the PEO process on aluminum," *Surface & Coatings Technology*, vol. 298, pp. 24-32, 2016.
- [20] D. O. Northwood, R. O. Hussein and X. Nie, "Environmentally Friendly Surface Treatment of Light Alloy Materials for Automotive Applications," in *The 18th International Corrosion Congress*, Perth, Australia, 2011.
- [21] K. Bobzin, F. Ernst, J. Zwick, T. Schlaefler, D. Cook, K. Nassenstein, A. Schwenk, F. Schreiber, T. Wenz, G. Flores and M. Hahn, "Coating Bores of Light Metal Engine Blocks with a Nanocomposite Material using the Plasma Transferred Wire Thermal Spray Process," *Journal of Thermal Spray Technology*, vol. 17, no. 3, pp. 344-351, 2008.
- [22] E. Lugscheider, R. Dicks, K. Kowalsky, D. Cook, K. Nassenstein and C. Verpoort, "A Materials System and Method of its Application for the Wear Protection of Aluminium Engine Cylinder Bore Surfaces," in *Proceedings of the International Thermal Spray Conference*, 2004.

- [23] Y. O. Oh, J. I. Mun and J. W. Kim, "Effects of alloying elements on microstructure and protective properties of Al₂O₃ coatings formed on aluminum alloy substrates by plasma electrolysis," *Surface Coating & Technology*, no. 240, pp. 141-148, 2009.
- [24] K. Tillous, T. Toll-Duchanoy, E. Bauer-Grosse, L. Hericher and G. Geandier, "Microstructure and phase composition of microarc oxidation surface layers formed on aluminium and its alloys," *Surface Coating & Technology*, no. 203, pp. 2969-2973, 2009.
- [25] R. O. Hussein and D. O. Northwood, "Improving the performance of magnesium alloys for automotive applications," *WIT Transactions on the Built*, vol. 137, p. 531-544, 2014.
- [26] R. O. Hussein, X. Nie and D. O. Northwood, "Plasma electrolytic oxidation (PEO) coatings on Mg-alloys for improved wear and corrosion resistance," *WIT Transactions on Engineering Sciences*, vol. 91, pp. 163-176, 2015.
- [27] R. O. Hussein, X. Nie and D. O. Northwood, "Production of high quality coatings on light alloys using Plasma Electrolytic Oxidation (PEO)," in *WIT Confrences*, La Certosa di Pontignano, 2016.
- [28] H. Duan, C. Yan and F. Wang, "Effect of electrolyte additives on performance of plasma electrolytic oxidation films formed on magnesium alloy AZ91D," *Electrochimica Acta*, vol. 52, pp. 3785-3793, 2007.
- [29] J. Curran and W. Clyne, "Thermo-physical properties of plasma electrolytic oxide coatings on aluminum," *Surface & Coatings Technology*, vol. 199, pp. 177-183, 2005.
- [30] R. O. Hussein, P. Zhang, D. O. Northwood and X. Nie, "Improving the Corrosion Resistance of Magnesium Alloy AJ62 by a Plasma Electrolytic Oxidation (PEO) Coating Process," *Corrosion and Materials*, vol. 36, no. 3, pp. 38-49, 2011.
- [31] A. L. Yerokhin, L. O. Snizhko, N. L. Gurevina, A. Leyland, A. Pilkington and A. Matthews, "Discharge characterization in plasma electrolytic oxidation of aluminium," *J. Phys. D Appl. Phys.*, no. 36, pp. 2110-2120, 2003.
- [32] R. O. Hussein, X. Nie and D. O. Northwood, "An investigation of ceramic coating growth mechanisms in plasma electrolytic oxidation (PEO) processing," *Electrochimica Acta*, vol. 112, pp. 111-119, 2013.
- [33] C. B. Wei, X. B. Tian, S. Q. Yang, X. B. Wang, R. Fu and P. K. Chu, "Anode current effects in plasma electrolytic oxidation," *Surface & Coatings Technology*, vol. 201, pp. 5021-5024, 2007.
- [34] R. O. Hussein, D. O. Northwood and X. Nie, "Processing-Microstructure Relationships in the Plasma Electrolytic Oxidation (PEO) Coating of a Magnesium Alloy," *Materials Sciences and Applications*, vol. 5, no. 3, pp. 124-139, 2014.

- [35] E. Cakmat, K. C. Tekin, U. Malsyooglu and S. Shrestha, "The effect of substrate composition on the electrochemical and mechanical properties of PEO coatings on Mg alloys," *Surface & Coatings Technology*, vol. 204, pp. 1305-1313, 2010.
- [36] R. O. Hussein, X. Nie and D. O. Northwood, "A spectroscopic and microstructural study of oxide coatings produced on a Ti-6Al-4V alloy by Plasma Electrolytic Oxidation," *J. of Materials Chemistry and Physics*, vol. 134, no. 1, pp. 484-492, 2012.
- [37] N. Yoshida, "Development of New I4 2.5L Gasoline Direct," SAE Technical Paper 2019-01-1199, 2019.
- [38] M. Hart, J. Gindele, T. Ramsteiner, G. Thater, B. Tschamon, M. Karres, B. Keiner and J. Fischer, "The New High-performance 4-cylinder Engine with Turbocharging from AMG," in *Internationales Wiener Motorensymposium*, Vienna, 2013.
- [39] S. Özer, E. Vural and S. Özel, "Effects of fusel oil use in a thermal coated engine," *Fuel*, vol. 306, 2021.
- [40] I. Arsie, A. Cricchio, C. Pianese, V. Ricciardi and M. D. Cesare, "Modeling Analysis of Waste Heat Recovery via Thermo-Electric Generator and Electric Turbo-Compound for CO2 Reduction in Automotive SI Engines," *Energy Procedia*, vol. 82, pp. 81-88, 2015.
- [41] J. Gao, G. Tian, A. Sorniotti, A. E. Karci and R. D. Palo, "Review of thermal management of catalytic converters to decrease engine emissions during cold start and warm up," *Applied Thermal Engineering*, vol. 147, pp. 177-187, 2019.
- [42] M. Andrie, S. Kokjohn, S. Paliwal, L. S. Kamo, A. Kamo and D. Procknow, "Low Heat Capacitance Thermal Barrier Coatings for Internal Combustion Engines," SAE International in United States, 2019.
- [43] Y. Wakisaka, M. Inayoshi, K. Fukui, H. Kosaka, Y. Hotta, A. Kawaguchi and e. al, "Reduction of Heat Loss and Improvement of Thermal Efficiency by Application of "Temperature Swing" Insulation to Direct-Injection Diesel Engines," *SAE Int. J. Engines*, vol. 9, no. 3, pp. 1449-1459, 2016.
- [44] A. Kawaguchi, H. Iguma, H. Yamashita, N. Takada, N. Nishikawa, C. Yamashita and e. al, "Thermo-Swing Wall Insulation Technology; - A Novel Heat Loss Reduction Approach on Engine Combustion Chamber," SAE International United States, 2016.
- [45] H. Kosaka, Y. Wakisaka, Y. Nomura, Y. Hotta, M. Koike and K. Nakakita, "Concept of "Temperature Swing Heat Insulation" in Combustion Chamber Walls, and Appropriate Thermo-Physical Properties for Heat Insulation Coat," *SAE Int. J. Engines*, vol. 1, no. 6, pp. 142-149, 2013.
- [46] K. Fukui, Y. Wakisaka, K. Nishikawa, Y. Hattori, H. Kosaka and A. Kawaguchi, "Development of Instantaneous Temperature Measurement Technique for Combustion

Chamber Surface and Verification of Temperature Swing Concept," SAE International United States, 2016.

- [47] L. E. Byrnes, L. L. VanKuiken Jr and M. S. Kramer, "High Pressure Water Jet Method of Blasting Low Density Metallic Surfaces". U.S. Patent 5380564, 10 Jan 1995.
- [48] J. A. Curran, T. Clyne, Y. Magurova and T. W. Clyne, "Mullite-rich Plasma Electrolytic Oxide Coatings for Thermal Barrier Applications," *Surface & Coatings Technology*, vol. 201, pp. 8683-8687, 2007.
- [49] J. A. Curran and T. W. Clyne, "Porosity in Plasma Electrolytic Oxide Coatings," *Acta Materialia*, vol. 54, pp. 1985-1993, 2005.
- [50] G. Borman and K. Nishiwaki, "Internal-combustion engine heat transfer," *Progress in Energy and Combustion Science*, vol. 13, no. 1, pp. 1-46, 1987.
- [51] "Enwin," [Online]. Available: <https://enwin.com/electric-rates-business/#nonrpp>. [Accessed 06 04 2022].
- [52] "CAS Software Reference Manual (for Pheonix)," A&D Technology, Inc, Ann Arbor.
- [53] U. Asad, *Engine Testing & Performance Cylinder Pressure Measurement*, Adobe Acrobat Reader, 2019.
- [54] J. B. Heywood, *Internal Combustion Engine Fundamentals*, The McGraw-Hill Companies, Inc., 1988.
- [55] M. J. Moran and H. N. Shapiro, *Fundamentals of Engineering Thermodynamics Fifth Edition*, Chichester, West Sussex, England: John Wiley & Sons, Inc., 2006.

APPENDIX

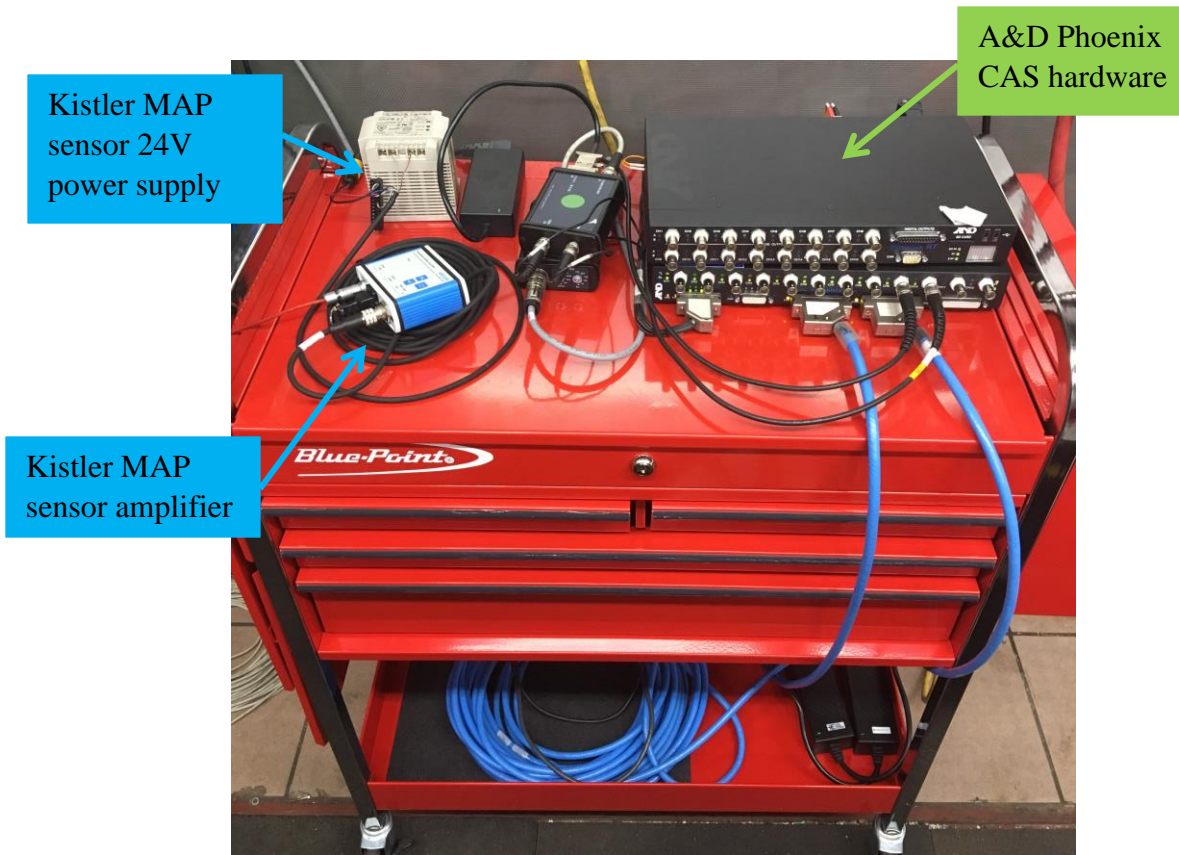


Figure A.30 - A&D Phoenix CAS hardware, Kistler MAP sensor amplifier and 24V power supply



Figure A.31 - AC Meiden dynamometer

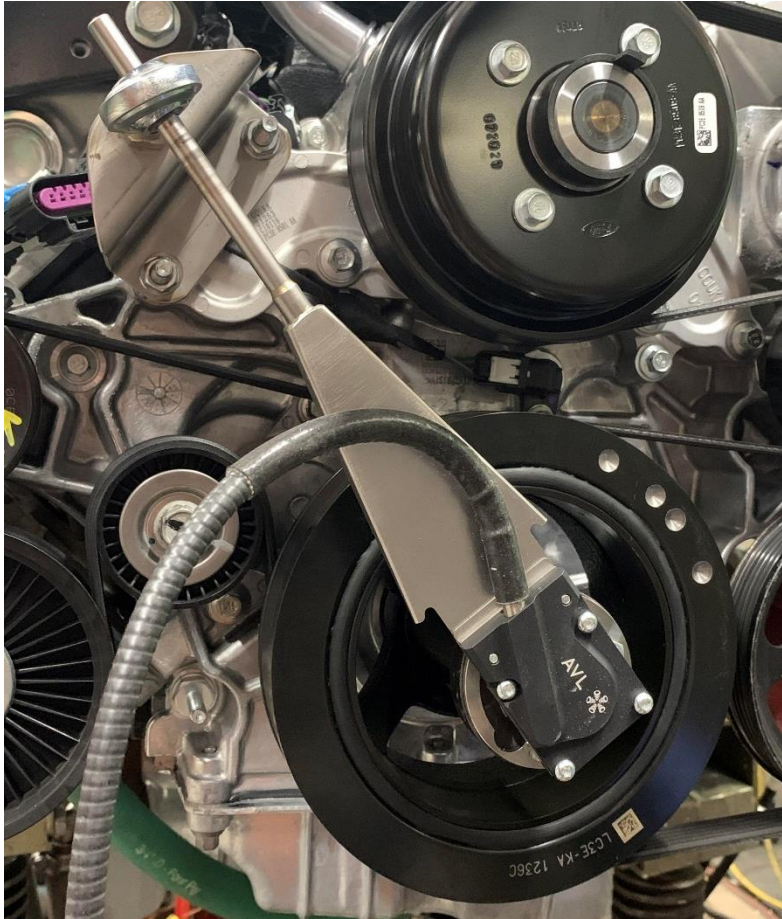


Figure A.32 - AVL encoder and mounting bracket

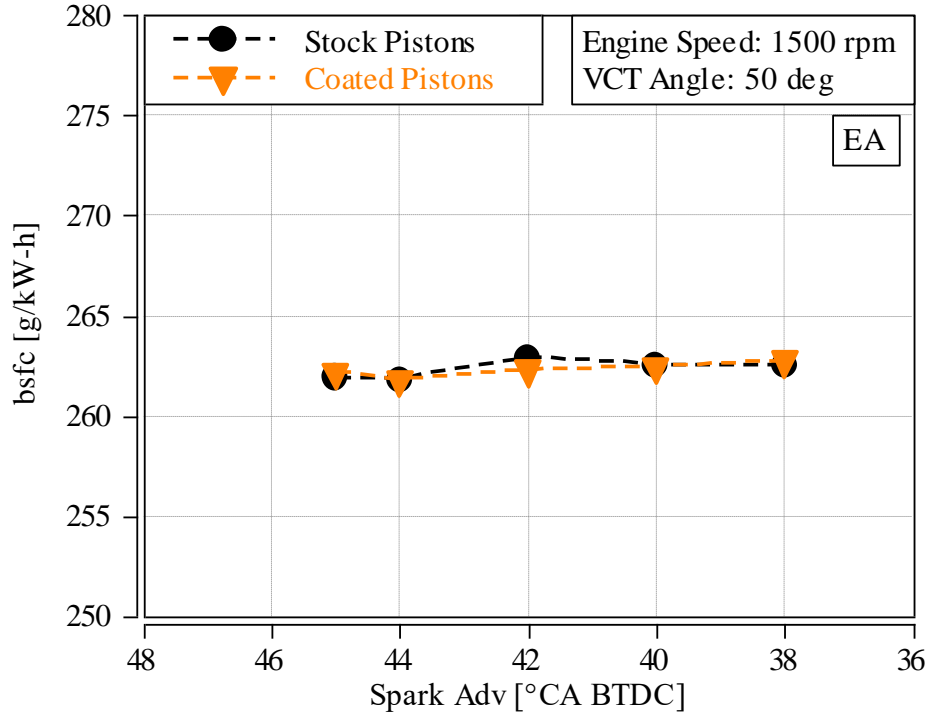


Figure A.33 - bsfc vs spark advance at 1500rpm 50° VCT retard

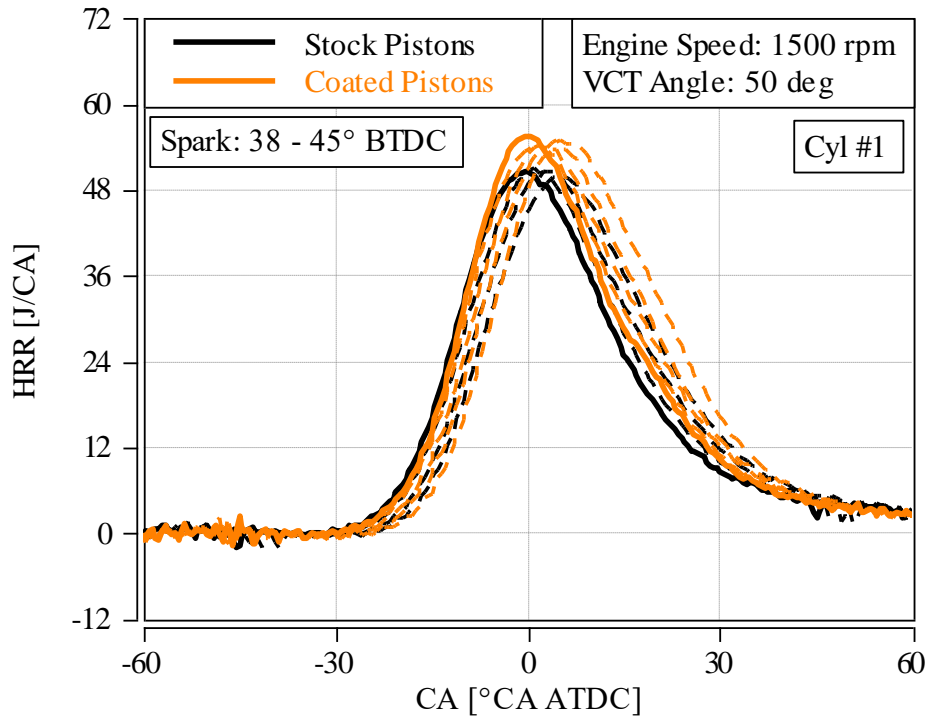


Figure A.34 - Heat Release Rate at 1500rpm 50° VCT retard spark sweep, Cylinder #1

Table A.6 - Steady-state results summary 1500rpm 50° VCT retard low load

Spark Adv [°CA BTDC]	Corrected Torque [Nm]	AFR	Throttle [%]	Exhaust Temperature [°C]	AM [kg/min]	Fuel Flow [kg/h]
45	262.4	14.4	21.7	544	2.58	10.8
45	263.3	14.3	21.6	556	2.59	10.8
44	262.5	14.4	21.7	557	2.58	10.8
44	263.2	14.3	21.6	556	2.59	10.8
42	262.2	14.3	21.7	560	2.58	10.8
42	263.0	14.4	21.6	558	2.59	10.8
40	262.3	14.3	21.7	563	2.58	10.8
40	263.2	14.3	21.6	561	2.60	10.8
38	262.5	14.3	21.7	566	2.58	10.8
38	263.0	14.4	21.6	563	2.60	10.9

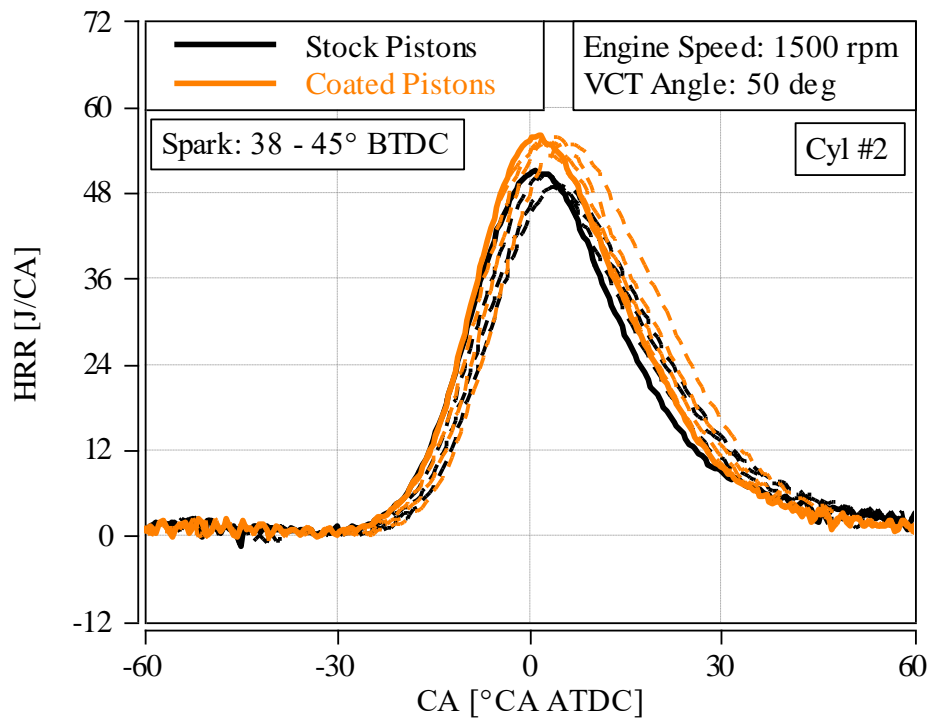


Figure A.35 - Heat Release Rate at 1500rpm 50° VCT retard spark sweep, Cylinder #2

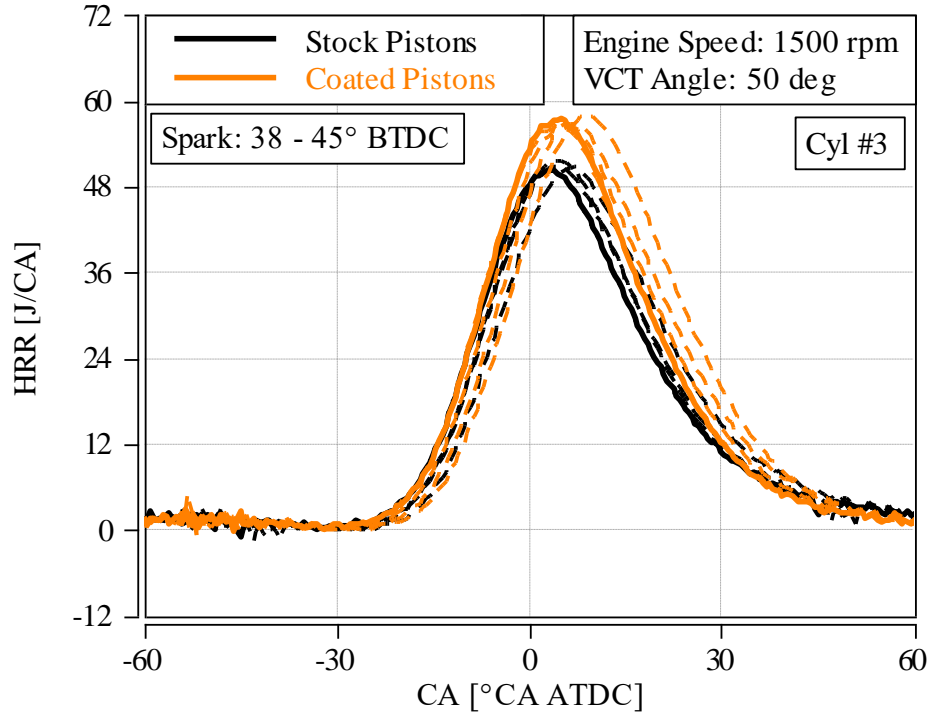


Figure A.36 - Heat Release Rate at 1500rpm 50° VCT retard spark sweep, Cylinder #3

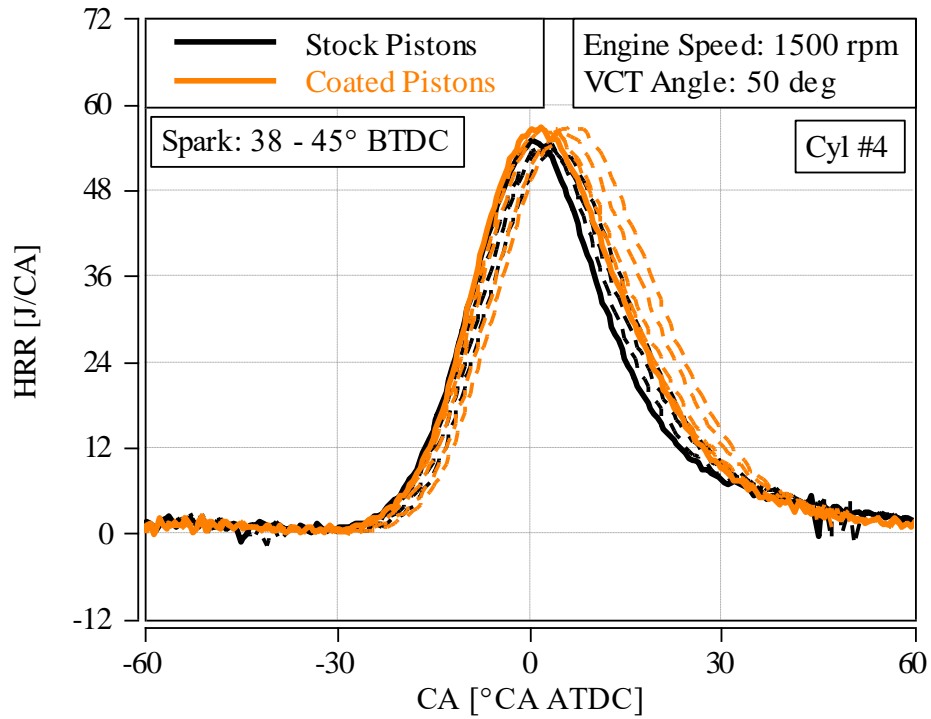


Figure A.37 - Heat Release Rate at 1500rpm 50° VCT retard spark sweep, Cylinder #4

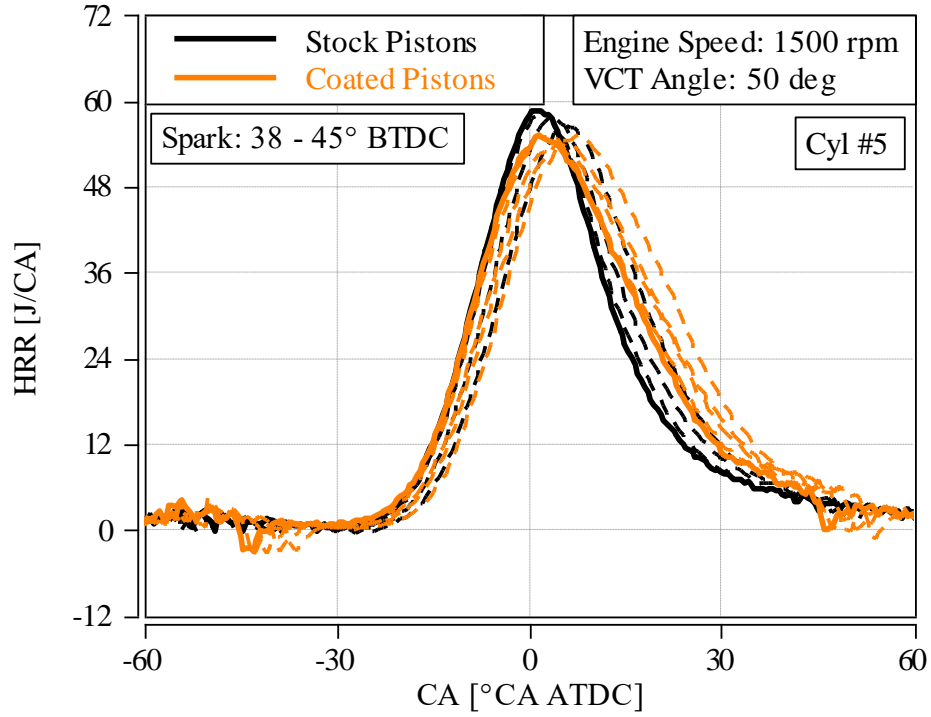


Figure A.38 - Heat Release Rate at 1500rpm 50° VCT retard spark sweep, Cylinder #5

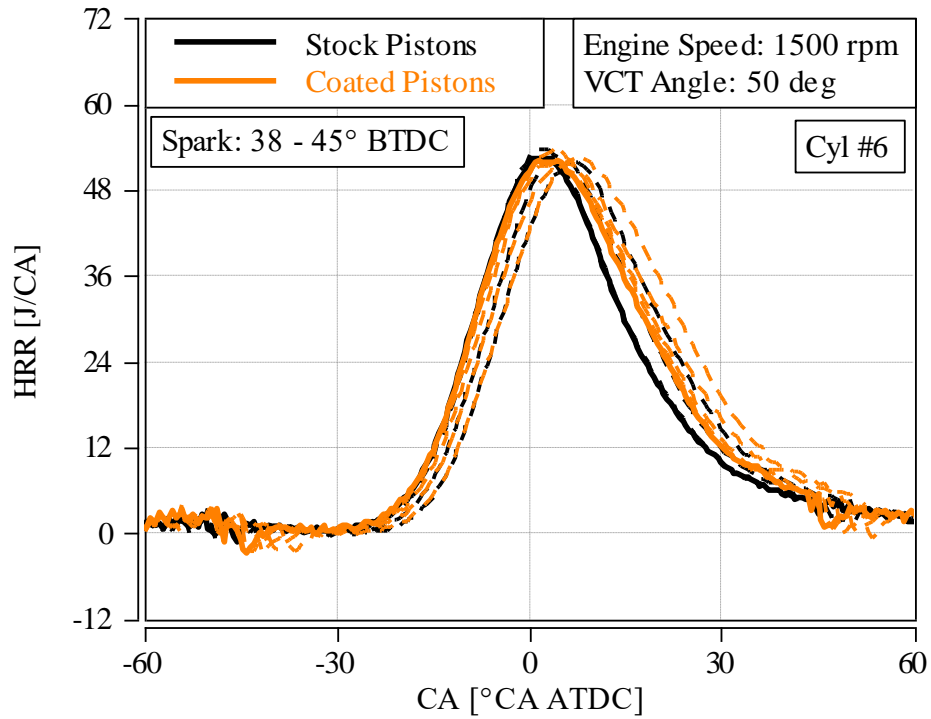


Figure A.39 - Heat Release Rate at 1500rpm 50° VCT retard spark sweep, Cylinder #6

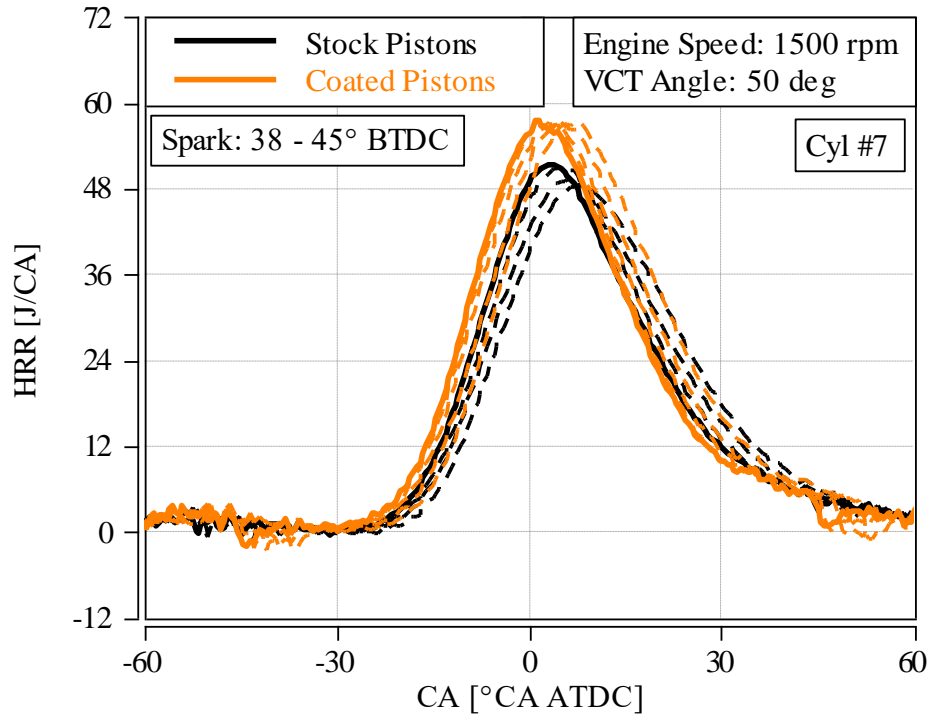


Figure A.40 - Heat Release Rate at 1500rpm 50° VCT retard spark sweep, Cylinder #7

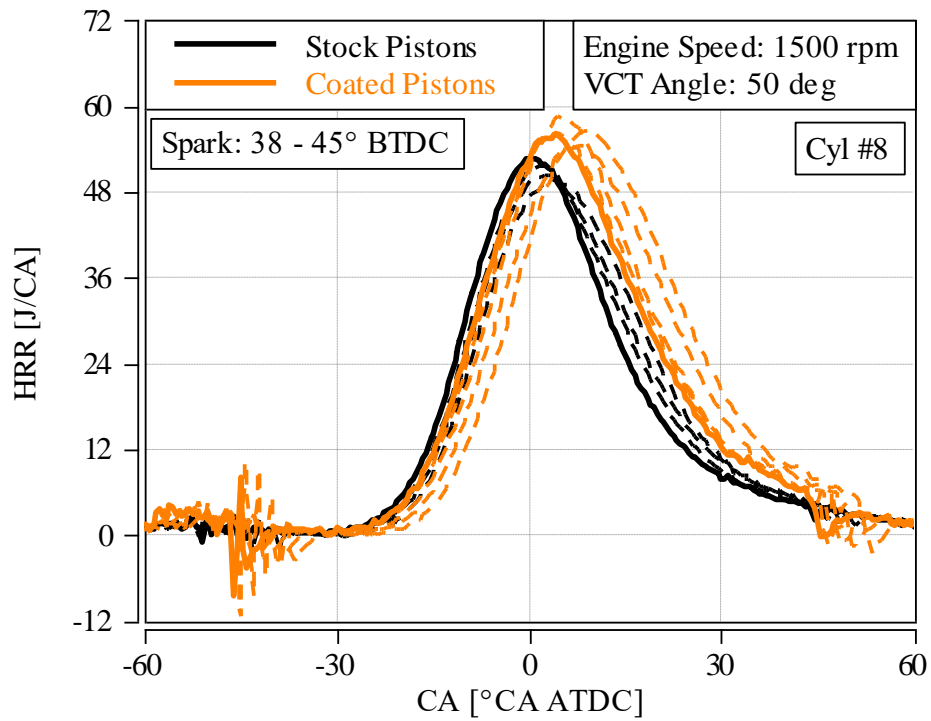


Figure A.41 - Heat Release Rate at 1500rpm 50° VCT retard spark sweep, Cylinder #8

VITA AUCTORIS

NAME: Brendon Bain

PLACE OF BIRTH: Toronto, Ontario, Canada